Westfälische
Wilhelms-Universität
Münster

Phase-field-crystal models for colloidal liquid crystals

Master thesis in physics

Daniel Lahrmann

February 2019

Supervisor:
Prof. Dr. Uwe Thiele
Institute of Theoretical Physics, Westfälische Wilhelms-Universität Münster
Prof. Dr. Raphael Wittkowski
Institute of Theoretical Physics, Westfälische Wilhelms-Universität Münster

Contents

1 Theoretical foundations

1.1 Functional derivative

A functional $\mathcal{F}[f]$ is an function of functions $f(\vec{r})$. One example of a functional is a integral of the form

$$\mathcal{F}[\rho] = \int \mathrm{d}\vec{r}\, g(\vec{r}, \rho(\vec{r})). \tag{1.1}$$

A functional derivative $\frac{\delta\mathcal{F}[\rho]}{\delta\rho(\vec{r})}$ is a general form of a directional derivative of a functional. For $\frac{\delta f(\vec{r}_i)}{\delta f(\vec{r})}$ it follows that

$$\frac{\delta\rho(\vec{r}_i)}{\delta\rho(\vec{r})} = \delta(\vec{r}_i - \vec{r}). \tag{1.2}$$

As for general derivatives, functional derivatives are linear and product and chain rule apply. For example the first functional derivative of the functional (1.1) is

$$\frac{\delta\mathcal{F}[\rho]}{\delta\rho(\vec{r}_0)} = \int \mathrm{d}\vec{r}\, \frac{\delta g(\vec{r}, \rho(\vec{r}))}{\delta\rho}\delta(\vec{r} - \vec{r}_0) = g'(\vec{r}_0, \rho(\vec{r}_0)) \tag{1.3}$$

with $g'(\vec{r}, \rho(\vec{r})) = \frac{\delta g(\vec{r}, \rho(\vec{r}))}{\delta\rho}$.

If the functional is defined on a fixed domain, it can be expressed in the form (here in 1D)

$$\int_a^b \mathrm{d}x F(\rho(x)) = \int_{-\infty}^{\infty} \mathrm{d}x\, F(\rho(x))\Theta(x - a)\Theta(b - x) \tag{1.4}$$

Using partial integration, it can be shown that

$$\int \mathrm{d}\vec{r}\, f(\vec{r})\vec{\nabla}^n\delta(\vec{r} - \vec{r}_0) = (-1)^n \int \mathrm{d}\vec{r}\, \left(\vec{\nabla}^n f(\vec{r})\right)\delta(\vec{r} - \vec{r}_0) = (-1)^n\vec{\nabla}^n f(\vec{r})\Big|_{\vec{r}=\vec{r}_0} \tag{1.5}$$

This will be needed in the following sections to derive the PFC equations.

1.2 Density functional theory

The classical density functional theory (DFT) describes an equilibrated many-particle system. To achieve this, the free-energy of the system has to be described as an functional of the density $\rho(\vec{r})$[1, 2]. A dynamic extension of this theory, the dynamical density functional theory (DDFT), can be used for a description of melting and freezing processes in colloidal systems.

First of all, the number density $\rho(\vec{r})$ at position $\vec{r}$ has to be defined. It is a measure of the probability to find a particle at $\vec{r}$. Consider a system with N particles. The position of particle i is $\vec{r}_i$. So the density can be expressed by

$$\rho_0(\vec{r}) = \left\langle \sum_{i=1}^{N} \delta(\vec{r} - \vec{r}_i) \right\rangle \tag{1.6}$$

where $\langle a \rangle$ is the grand-canonical ensemble average of a. If $\Xi = \mathrm{tr}(\exp(-\beta(H - \mu N)))$ is the grand-canonical partition function, with the hamilton-function H, the particle number N and the chemical potential μ, $\Omega = -k_\mathrm{B} T \ln(\Xi)$ is the grand-canonical potential. One important property of the grand-canonical potential is, that it is minimal if the density is equilibrated

$$\frac{\delta\Omega\left(T, \mu, [\rho(\vec{r})]\right)}{\delta\rho(\vec{r}')} = 0. \tag{1.7}$$

This potential is not known exactly and depends on the properties of the particles. With a Legendre-transformation the grand-canonical potential can be expressed by the free-energy functional $\mathcal{F}[\rho]$:

$$\Omega\left(T, \mu, [\rho(\vec{r})]\right) = \mathcal{F}\left(T, \mu, [\rho(\vec{r})]\right) - \mu \int \mathrm{d}\vec{r}\rho(\vec{r}) \tag{1.8}$$

The free energy can be split into an ideal part $\mathcal{F}_\mathrm{id}$, an external part $\mathcal{F}_\mathrm{ext}$ and an excess part $\mathcal{F}_\mathrm{exc}$ [3].

$$\mathcal{F}(T, [\rho(\vec{r})]) = \mathcal{F}_\mathrm{id}(T, [\rho(\vec{r})]) + \mathcal{F}_\mathrm{ext}(T, [\rho(\vec{r})]) + \mathcal{F}_\mathrm{exc}(T, [\rho(\vec{r})]) \tag{1.9}$$

The ideal term is the entropic part. It can be expressed by

$$\mathcal{F}_\mathrm{id}(T, [\rho(\vec{r})]) = k_\mathrm{B} T \int \mathrm{d}\vec{r}\rho(\vec{r})[\ln(\Lambda^d \rho(\vec{r})) - 1]. \tag{1.10}$$

Here k_B is the Boltzmann constant, T the temperature, d the considered spatial dimension and Λ the de-Broglie wavelength. The interaction between the external field $U(\vec{r})$ and the density has the form:

$$\mathcal{F}_\mathrm{ext}(T, [\rho(\vec{r})]) = \int \mathrm{d}\vec{r}\rho(\vec{r}) U_\mathrm{ext}(\vec{r}) \tag{1.11}$$

The final term in (1.9) describes the interaction between the particles. A formally exact expression for $\mathcal{F}_{\text{exc}}$ can be obtained by a functional Taylor expansion about a homogeneous density ρ_{ref}[4]. With $\Delta\rho = \rho - \rho_{\text{ref}}$ it follows

$$\mathcal{F}_{\text{exc}}(T, [\rho(\vec{r})]) = \mathcal{F}^{(0)}_{\text{exc}}(T, [\rho(\vec{r})]) + \lim_{N\to\infty} k_{\text{B}}T \sum_{n=1}^{N} \frac{1}{n!} \mathcal{F}^{(n)}_{\text{exc}}(T, [\rho(\vec{r})]) \tag{1.12}$$

with

$$\mathcal{F}^{(n)}_{\text{exc}}(T, [\rho(\vec{r})]) = -\int \mathrm{d}\vec{r}_1 ... \mathrm{d}\vec{r}_n c^{(n)}(\vec{r}_1, ..., \vec{r}_n) \prod_{i=1}^{n} \Delta\rho(\vec{r}_i) \tag{1.13}$$

$c^{(n)}$ is the direct correlation function of n-th order, and is given by

$$c^{(n)}(\vec{r}_1, ..., \vec{r}_n) = -\beta \left. \frac{\delta^n \mathcal{F}_{\text{exc}}}{\delta\rho(\vec{r}_1)...\delta\rho(\vec{r}_n)} \right|_{\rho_{\text{ref}}} = c^{(n)}(\vec{r}_2 - \vec{r}_1, ..., \vec{r}_n - \vec{r}_1) \tag{1.14}$$

Here $\beta = \frac{1}{k_{\text{B}}T}$. The constant zeroth-order contribution in (1.12) is irrelevant and the first order contribution is zero.

Because the system is translation-invariant it follows, that the correlation can brought into the form $c^{(n)}(\vec{r}_1, ..., \vec{r}_n) = c^{(n)}(\vec{r}_2 - \vec{r}_1, ..., \vec{r}_n - \vec{r}_1)$. Then, the integral over the spatial variables $\vec{r}_2, ..., \vec{r}_n$ in Eq. (1.13) becomes a convolution of the correlation function and the density-differences $\Delta\rho(\vec{r}_i)$.

1.3 Dynamical density functional theory

If the equilibrated density $\rho(\vec{r})$ is perturbed, the free energy will normally not be minimal anymore. The resulting changes in time can be described by the dynamical density functional theory (DDFT). The basic equation of DDFT is the continuity equation [2]:

$$\partial_t \rho = -\nabla \cdot \vec{j} = D_T \vec{\nabla} \cdot \left(\rho \vec{\nabla} \frac{\delta \mathcal{F}[\rho]}{\delta \rho} \right) \tag{1.15}$$

i.e. the dynamics conserves the particle number. D_T is the diffusion constant.

The DDFT describes on a diffusive timescale the motion of Brownian particles, i.e. particles, which move in a viscose medium and collide stochastically. The functional derivative can be interpreted as an inhomogeneous chemical potential $\mu(\vec{r})$, i.e. the flux $\vec{j}$ is driven by the gradient of μ.

The DDFT equation can be derived from a Smoluchowski equation [5]. To do this, the time dependent correlation functions have to be expressed by equilibrium correlation functions.

With the free energy functionals known from DFT, the DDFT equation has the form:

$$\partial_t \rho(\vec{r},t) = D_T \left\{ k_\mathrm{B}T \triangle \rho(\vec{r},t) + \vec{\nabla} \left[\rho(\vec{r},t) \vec{\nabla} \left(U_\mathrm{ext} \right.\right.\right. \\ \left.\left.\left. -k_\mathrm{B}T \lim_{N\to\infty} \sum_{n=2}^{N} \int \mathrm{d}\vec{r}_1 ... \mathrm{d}\vec{r}_n \left(\prod_{i=1}^{n} \rho(\vec{r}_i) \right) c^{(n)}(\vec{r}_2 - \vec{r}_1, ..., \vec{r}_n - \vec{r}_1) \left(\sum_{i=1}^{n} \frac{\delta(\vec{r} - \vec{r}_i)}{\rho(\vec{r}_i)} \right) \right) \right] \right\} \tag{1.16}$$

1.4 Derivation of a non liquid-crystal PFC model

The PFC is an approximated form of the DDFT. It describes the density field in a less precise way, for example neglecting high Fourier modes for the crystal. So the basic structure of the crystal is kept, but some details are lost. The PFC model can be derived from DDFT in two ways.

1.4.1 First way of derivation

The first scheme is described in Ref. [2] and is sketched next.

First, a order-parameter field $\psi(\vec{r},t)$ is introduced, which describes the relative density deviation

$$\rho(\vec{r},t) = \rho_\mathrm{ref} \left(1 + \psi(\vec{r},t)\right), \tag{1.17}$$

i.e. $\Delta\rho = \rho_\mathrm{ref}\psi$, where one assumes, that $|\psi| < 1$. Now the basic steps for the derivation of the PFC model are:

1. insert $\rho(\vec{r},t)$ from (1.17) into the free-energy functional
2. Taylor expand the functional (1.9) in terms of power of $\psi(\vec{r},t)$
3. use a gradient expansion of the excess free energy (1.13)
4. insert the solution into the DDFT equation (1.16)

The external part of the functional has the form

$$\mathcal{F}_\mathrm{ext}(T, [\psi(\vec{r})]) = \rho_\mathrm{ref} \int \mathrm{d}\vec{r}(1 + \psi(\vec{r})) U_\mathrm{ext}(\vec{r}) = F^0_\mathrm{ext} + \rho_\mathrm{ref} \int \mathrm{d}\vec{r}\psi(\vec{r}) U_\mathrm{ext}(\vec{r}) \tag{1.18}$$

where $F^0_\mathrm{ext} = \int \mathrm{d}\vec{r}\rho_\mathrm{ref} U_\mathrm{ext}(\vec{r})$ is an irrelevant constant.

The ideal free energy part is Taylor expanded and becomes:

$$\begin{aligned}\mathcal{F}_{\mathsf{id}}(T,[\psi(\vec{r})]) &= k_{\mathsf{B}}T\int \mathrm{d}\vec{r}\rho_{\mathsf{ref}}(1+\psi(\vec{r}))[\ln(\Lambda^d\rho_{\mathsf{ref}}(1+\psi(\vec{r}))-1] \\ &= k_{\mathsf{B}}T\int \mathrm{d}\vec{r}\rho_{\mathsf{ref}}[\ln(\Lambda^d\rho_{\mathsf{ref}})-1] + k_{\mathsf{B}}T\int \mathrm{d}\vec{r}\rho_{\mathsf{ref}}\ln(\Lambda^d\rho_{\mathsf{ref}})\psi(\vec{r}) \\ &+ k_{\mathsf{B}}T\lim_{N\to\infty}\int \mathrm{d}\vec{r}\rho_{\mathsf{ref}}\sum_{n=2}^{N+2}\frac{(-\psi(\vec{r}))^n}{n(n-1)}\end{aligned} \tag{1.19}$$

The n-th term of the excess part of the energy functional has the form:

$$\mathcal{F}^{(n)}_{\mathsf{exc}}(T,[\psi(\vec{r})]) = -\rho^n_{\mathsf{ref}}\int \mathrm{d}\vec{r}_1...\mathrm{d}\vec{r}_n c^{(n)}(\vec{r}_2-\vec{r}_1,...,\vec{r}_n-\vec{r}_1)\prod_{i=1}^{n}\psi(\vec{r}_i) \tag{1.20}$$

The included $n-1$ convolutions of this term can be computed using Fourier transformation:

$$\int \mathrm{d}\vec{r}_2...\mathrm{d}\vec{r}_n c^{(n)}(\vec{r}_2-\vec{r}_1,...,\vec{r}_n-\vec{r}_1)\prod_{i=2}^{n}\psi(\vec{r}_i) = \mathfrak{F}^{-1}\left(\sqrt{2\pi}^{d(n-1)}\tilde{c}^{(n)}(\vec{k}_2,...,\vec{k}_n)\prod_{i=2}^{n}\tilde{\psi}(\vec{k}_i)\right) \tag{1.21}$$

The Fourier transformed correlation function can be Taylor expanded multidimensionally around $(\vec{k}_2,...,\vec{k}_n) = 0$:

$$\tilde{c}^{(n)}(\underline{k}) = \frac{1}{\sqrt{2\pi}^{d(n-1)}}\int \mathrm{d}\underline{r}c^{(n)}(\underline{r})\exp(-i\underline{r}\underline{k}) = \frac{1}{\sqrt{2\pi}^{d(n-1)}}\lim_{N\to\infty}\sum_{|\alpha|=0}^{N+2-n}\frac{\underline{k}^\alpha}{\alpha!}\frac{\partial^{|\alpha|}\tilde{c}^{(n)}(\underline{k})}{\partial\underline{k}^\alpha}\bigg|_{\underline{k}=0} \tag{1.22}$$

Here $\underline{k}$ is defined as a vector in the form $\underline{k} = (\vec{k}_2,...,\vec{k}_n)$. $\alpha_{(i,m)}$ is an arbitrary positive integer representing an index for particle i in the coordinate direction m. α is a multi-index and includes all $\alpha_{(i,m)} \in \mathbb{N}^0$ [1] with $2 \leq i \leq n$ and $m \leq d$ (all $\alpha_{(1,m)}$ are defined as 0). $|\alpha|$ is the sum of all $\sum_{m=1}^{d}\sum_{i=2}^{n}\alpha_{(i,m)}$ and $\alpha! = \prod_{m=1}^{d}\prod_{i=2}^{n}\alpha_{(i,m)}!$. $\underline{k}^\alpha$ is defined by $\underline{k}^\alpha = \prod_{m=1}^{d}\prod_{i=2}^{n}k_{(i,m)}^{\alpha_{(i,m)}}$. The derivatives $\frac{\partial^{|\alpha|}}{\partial\underline{k}^\alpha}$ are defined as $\frac{\partial^{|\alpha|}}{\partial\underline{k}^\alpha} = \prod_{m=1}^{d}\prod_{i=2}^{n}\frac{\partial^{\alpha(i,m)}}{\partial k_{(i,m)}^{\alpha(i,m)}}$. The sum $\sum_{|\alpha|=0}^{N}$ is equal to $\prod_{m=1}^{d}\prod_{i=2}^{n}\sum_{\alpha_{(i,m)}}\Theta(N-|\alpha|)$. So for a 2d system for the three particle correlation function $(n=3)$ we have

[1] $\mathbb{N}^0$ is the set of all natural numbers including 0

$$
\begin{aligned}
\underline{k} &= (k_{2,x}, k_{2,y}, k_{3,x}, k_{3,y}) \\
\alpha &= (\alpha_{2,x}, \alpha_{2,y}, \alpha_{3,x}, \alpha_{3,y}) \\
\underline{k}^{\alpha} &= k_{2,x}^{\alpha_{(2,x)}} \cdot k_{2,y}^{\alpha_{(2,y)}} \cdot k_{3,x}^{\alpha_{(3,x)}} \cdot k_{3,y}^{\alpha_{(3,y)}} \\
|\alpha| &= \alpha_{(2,x)} + \alpha_{(2,y)} + \alpha_{(3,x)} + \alpha_{(3,y)} \\
\alpha! &= \alpha_{(2,x)}!\alpha_{(2,y)}!\alpha_{(3,x)}!\alpha_{(3,y)}! \\
\frac{\partial^{|\alpha|}}{\partial \underline{k}^{\alpha}} &= \frac{\partial^{\alpha_{(2,x)}}}{\partial k_{2,x}^{\alpha_{(2,x)}}} \frac{\partial^{\alpha_{(2,y)}}}{\partial k_{2,y}^{\alpha_{(2,y)}}} \frac{\partial^{\alpha_{(3,x)}}}{\partial k_{3,x}^{\alpha_{(3,x)}}} \frac{\partial^{\alpha_{(3,y)}}}{\partial k_{3,y}^{\alpha_{(3,y)}}} \\
\sum_{|\alpha|=0}^{N} &= \sum_{\alpha_{(2,x)}=0}^{N} \sum_{\alpha_{(2,y)}=0}^{N-\alpha_{(2,x)}} \sum_{\alpha_{(3,x)}=0}^{N-\alpha_{(2,x)}-\alpha_{(2,y)}} \sum_{\alpha_{(3,y)}=0}^{N-\alpha_{(2,x)}-\alpha_{(2,y)}-\alpha_{(3,x)}}
\end{aligned}
$$

Using (1.22), the derivative of the transformed correlation function can be computed as

$$
\left.\frac{\partial^{|\alpha|}\tilde{c}^{(n)}(\underline{k})}{\partial \underline{k}^{|\alpha|}}\right|_{\underline{k}=0} = \frac{1}{\sqrt{2\pi}^{d(n-1)}} \int \mathrm{d}\underline{r}\, (-i)^{|\alpha|} \underline{r}^{\alpha} c^{(n)}(\underline{r}) = \frac{(-i)^{|\alpha|}}{\sqrt{2\pi}^{d(n-1)}} A_{\alpha}^{(n)} \tag{1.23}
$$

where the moments $A_{\alpha}^{(n)}$ are defined as the integrals

$$
A_{\alpha}^{(n)} = \int \mathrm{d}\underline{r}\, \underline{r}^{\alpha} c^{(n)}(\underline{r}) \tag{1.24}
$$

In this way the Fourier transformed correlation function is expressed as a power series. After multiplying this series with the product of all $\psi(\vec{r}_i)$ except $\psi(\vec{r}_1)$, and back-transforming the expression of equation (1.21), the excess energy part of the n-th order becomes:

$$
\mathcal{F}_{\mathsf{exc}}(T, [\psi(\vec{r})]) = -k_{\mathsf{B}} T \lim_{N\to\infty} \sum_{n=2}^{N+2} \frac{\rho_{\mathsf{ref}}^n}{n!} \int \mathrm{d}\vec{r} \psi(\vec{r}) \sum_{|\alpha|=0}^{N+2-n} \frac{(-1)^{|\alpha|}}{\alpha!} A_{\alpha}^{(n)} \prod_{j=2}^{n} \left(\prod_{m=1}^{d} \partial_{x_m}^{\alpha_{(j,m)}} \psi(\vec{r}) \right) \tag{1.25}
$$

With these terms the functional derivative of the free energy with respect to ψ has the form:

$$
\begin{aligned}
\frac{\delta \mathcal{F}(T, [\psi(\vec{r})])}{\delta \psi(\vec{r}')} =& \rho_{\mathsf{ref}} k_B T \left(\ln(\Lambda^3 \rho_{\mathsf{ref}}) - \lim_{N\to\infty} \sum_{n=1}^{N+1} \frac{(-\psi)^n}{n} \right) + \rho_{\mathsf{ref}} U_{\mathsf{ext}}(\vec{r}') \\
& - k_B T \rho_{\mathsf{ref}} \lim_{N\to\infty} \sum_{n=1}^{N+1} \frac{\rho_{\mathsf{ref}}^n}{(n+1)!} \sum_{|\alpha|=0}^{N+1-n} \frac{(-1)^{|\alpha|}}{\alpha!} A_{\alpha}^{(n+1)} \sum_{i=1}^{n} \left(\prod_{m=1}^{d} (-\partial_{x_m})^{\alpha_{(i,m)}} \right) \prod_{i\neq j} \left(\prod_{m=1}^{d} \partial_{x_m}^{\alpha_{(j,m)}} \psi(\vec{r}') \right)
\end{aligned} \tag{1.26}
$$

Before the PFC equation can be obtained, the DDFT equation (1.15) has to be reformulated. Due to the form of the density, the functional derivative with respect to ρ can be reformulated as a functional derivative with respect to ψ:

$$\frac{\delta \mathcal{F}(T,[\rho(\vec{r})])}{\delta \rho(\vec{r'})} = \frac{1}{\rho_{\mathsf{ref}}} \frac{\delta \mathcal{F}(T,[\psi(\vec{r})])}{\delta \psi(\vec{r'})} \tag{1.27}$$

Dividing the DDFT equation (1.15) by ρ_{ref} the PFC equation becomes

$$\partial_t \psi = \frac{D_T}{\rho_{\mathsf{ref}}} \nabla \left[(1+\psi) \nabla \frac{\delta \mathcal{F}(T,[\psi(\vec{r})])}{\delta \psi(\vec{r'})} \right] \tag{1.28}$$

With the variation (1.26) the PFC equation finally is

$$\begin{aligned} \partial_t \psi =& D_T \lim_{N\to\infty} \nabla \Bigg[(1+\psi) \nabla \Bigg(-k_{\mathsf{B}} T \sum_{n=1}^{N+1} \frac{(-\psi)^n}{n} + U_{\mathsf{ext}}(\vec{r}) \\ & -k_{\mathsf{B}} T \sum_{n=1}^{N+1} \frac{\rho_{\mathsf{ref}}^n}{(n+1)!} \sum_{|\alpha|=0}^{N+1-n} \frac{(-1)^{|\alpha|}}{\alpha!} A_\alpha^{(n+1)} \sum_{i=1}^{n} \left(\prod_{m=1}^{d} (-\partial_{x_m})^{\alpha_{(i,m)}} \right) \prod_{i\neq j} \left(\prod_{m=1}^{d} \partial_{x_m}^{\alpha_{(j,m)}} \psi(\vec{r}) \right) \Bigg) \Bigg] \end{aligned} \tag{1.29}$$

If $N \neq \infty$ one obtain the PFC equation of order N.

1.4.2 Second way of derivation

In the second way the DDFT equation is approximated directly. The basic steps are:

1. insert the ansatz (1.17) for $\rho(\vec{r},t)$ into the DDFT equation (1.16)
2. perform a gradient expansion of the excess part

The main advantage of this method is, that the ideal part is not approximated and remains exact, one obtains more exact solutions. Compared to the results (1.29) of the first way only the ideal part is changed, and the resulting PFC equation of order N is

$$\begin{aligned} \partial_t \psi =& k_{\mathsf{B}} T D_T \triangle \psi + D_T \nabla \Bigg[(1+\psi) \nabla \Bigg(U_{\mathsf{ext}}(\vec{r}) \\ & -k_{\mathsf{B}} T \sum_{n=1}^{N+1} \frac{\rho_{\mathsf{ref}}^n}{(n+1)!} \sum_{|\alpha|=0}^{N+1-n} \frac{(-1)^{|\alpha|}}{\alpha!} A_\alpha^{(n+1)} \sum_{i=1}^{n} \left(\prod_{m=1}^{d} (-\partial_{x_m})^{\alpha_{(i,m)}} \right) \prod_{i\neq j} \left(\prod_{m=1}^{d} \partial_{x_m}^{\alpha_{(j,m)}} \psi(\vec{r}) \right) \Bigg) \Bigg] \end{aligned} \tag{1.30}$$

Here the definition of the order is similar to the definition of the order in (1.29).

From here onwards, only the two particle correlation function (i.e. the pair correlation function) will be considered. This is known as the Ramakrishnan-Yussouff approximation[4]. Because only the pair correlation function is considered, all indexes have the form $\alpha_{(2,m)}$. To simplify the following equations, the 2 will be dropped ($\alpha_m = \alpha_{(2,m)}$). If the pair correlation function $c^{(2)}(\vec{r}_2 - \vec{r}_1)$ only depends on the distance $|\vec{r}_2 - \vec{r}_1| = r$, and the integrals can be split in a dimension independent part $A^{(2)}_{u,r} = \int_0^\infty \mathrm{d}r\, r^u c^{(2)}(r)$ and the integrals over the angles. Therefor the integrals will be solved in spherical coordinates of dimension N. So for 2D follows

$$\begin{pmatrix} x \\ y \end{pmatrix} = r \begin{pmatrix} \cos\varphi \\ \sin\varphi \end{pmatrix} \tag{1.31}$$

$$\int_{-\infty}^{\infty} \mathrm{d}x \int_{-\infty}^{\infty} \mathrm{d}y\, f(x,y) = \int_0^\infty \mathrm{d}r \int_0^{2\pi} \mathrm{d}\varphi\, r f(r,\varphi) \tag{1.32}$$

and for 3D

$$\begin{pmatrix} x \\ y \\ z \end{pmatrix} = r \begin{pmatrix} \cos\varphi \sin\vartheta \\ \sin\varphi \sin\vartheta \\ \cos\vartheta \end{pmatrix} \tag{1.33}$$

$$\int_{-\infty}^{\infty} \mathrm{d}x \int_{-\infty}^{\infty} \mathrm{d}y \int_{-\infty}^{\infty} \mathrm{d}z\, f(x,y,z) = \int_0^\infty \mathrm{d}r \int_0^{\pi} \mathrm{d}\vartheta \int_0^{2\pi} \mathrm{d}\varphi\, r^2 \sin\vartheta f(r,\vartheta,\varphi) \tag{1.34}$$

The integral over the angle becomes 0 if at least one index α_i is odd (the same applies to the 1D case). If all indexes are even the integral over the angle in the 2D case has the solution

$$\int_0^{2\pi} \mathrm{d}\varphi \cos^{2m}(\varphi) \sin^{2n}(\varphi) = 2\frac{\Gamma\left(n+\frac{1}{2}\right)\Gamma\left(m+\frac{1}{2}\right)}{\Gamma(n+m+1)} \tag{1.35}$$

and the solution in the 3D case is

$$\int_0^{\pi} \mathrm{d}\vartheta \int_0^{2\pi} \mathrm{d}\varphi \cos^{2m}(\varphi) \sin^{2n}(\varphi) \sin^{2n+2m+1}\vartheta \cos^{2o}\vartheta = 2\frac{\Gamma\left(n+\frac{1}{2}\right)\Gamma\left(m+\frac{1}{2}\right)\Gamma\left(o+\frac{1}{2}\right)}{\Gamma\left(n+m+o+\frac{3}{2}\right)} \tag{1.36}$$

$\Gamma(x)$ is the Gamma function. With $\Gamma\left(\frac{1}{2}\right) = \sqrt{\pi}$ and $\Gamma(x+1) = x\Gamma(x)$, $\Gamma\left(n+\frac{1}{2}\right)$ became

$$\Gamma\left(n+\frac{1}{2}\right) = \frac{\sqrt{\pi}(2n)!}{4^n n!} \tag{1.37}$$

So the moments for the 1D-3D cases can be rewritten in the form

$$A^{(2)}_{\alpha_x} = 2A^{(2)}_{|\alpha|,r} \tag{1.38a}$$

$$A^{(2)}_{\alpha_x,\alpha_y} = \frac{2\pi\alpha_x!\alpha_y!}{2^{\alpha_x+\alpha_y}\left(\frac{\alpha_x}{2}\right)!\left(\frac{\alpha_y}{2}\right)!\left(\frac{|\alpha|}{2}\right)!}A^{(2)}_{|\alpha|+1,r} \tag{1.38b}$$

$$A^{(2)}_{\alpha_x,\alpha_y,\alpha_z} = \frac{8\pi\alpha_x!\alpha_y!\alpha_z!\left(\frac{|\alpha|+2}{2}\right)!}{\left(\frac{\alpha_x}{2}\right)!\left(\frac{\alpha_y}{2}\right)!\left(\frac{\alpha_z}{2}\right)!(|\alpha|+2)!}A^{(2)}_{|\alpha|+2,r} \tag{1.38c}$$

Next, these moments will be plugged into the excess part. Then the terms will be sorted by $|\alpha|$, and the sum over all α_m with $|\alpha| = 2\mu$ is rewritten in a binodal form for the partial derivative $\partial_m^{\alpha_m}$. With (1.38b) for the 2D case it follows that

$$\begin{aligned}\sum_{|\alpha|=0}^{M}\frac{2\pi}{4^{|\alpha|}\alpha_x!\alpha_y!|\alpha|!}A^{(2)}_{2|\alpha|+1,r}\partial_x^{2\alpha_x}\partial_y^{2\alpha_y}\psi(\vec{r}) &= \sum_{\mu=0}^{M}\frac{2\pi}{4^{\mu}(\mu!)^2}A^{(2)}_{2\mu+1,r}\sum_{\alpha_x=0}^{\mu}\frac{\mu!}{\alpha_x!(\mu-\alpha_x)!}\partial_x^{2\alpha_x}\partial_y^{2(\mu-\alpha_x)}\psi(\vec{r}) \\ &= \sum_{\mu=0}^{M}\frac{2\pi}{4^{\mu}(\mu!)^2}A^{(2)}_{2\mu+1,r}\triangle^{\mu}\psi(\vec{r}).\end{aligned} \tag{1.39}$$

Here $2M = N$ and $\triangle$ is the laplace operator. A similar expression follows for the 3D case. As a result, the PFC equation (1.30) for rotational symmetric particles has the form

$$\partial_t\psi = k_{\mathsf{B}}TD_T\triangle\psi + D_T\nabla\left[(1+\psi)\nabla\left(U_{\mathsf{ext}}(\vec{r}) - k_{\mathsf{B}}T\rho_{\mathsf{ref}}\sum_{\mu=0}^{M}\tilde{A}^{(2)}_{2\mu,r}\triangle^{\mu}\psi(\vec{r})\right)\right] \tag{1.40}$$

The prefactor $\tilde{A}^{(2)}_{2\mu,r}$ contains $A^{(2)}_{u,r}$ and constants which depend on μ and the dimension of the system. They can be derived by using the equations (1.38a)-(1.38c) and considering the binomial form of the excess part. The terms are given in table 1.1. The same follows also for the PFC equation derived with the first scheme (1.30).

dimension	$\tilde{A}^{(2)}_{2\mu,r}$
1D	$\frac{2}{(2\mu)!}A^{(2)}_{2\mu,r}$
2D	$\frac{2\pi}{(\mu!)^2 4^{\mu}}A^{(2)}_{2\mu+1,r}$
3D	$\frac{8\pi(\mu+1)}{(2\mu+2)!}A^{(2)}_{2\mu+2,r}$

Table 1.1: Dependence of $\tilde{A}^{(2)}_{2\mu,r}$ on the dimension of the system

1.5 Continuation

[6–8]

One important property of a non linear differential equation are the fixed points of this equation (here $\partial_t \psi = \vec{G}(\vec{x}, \lambda) = 0$) for a free parameter λ. To find this multidimensional root, the Newton method can be used.

To find the root of a system of N equation $\vec{f}(\vec{x}) : \mathbb{R}^N \to \mathbb{R}^N$, $\vec{f}(\vec{x})$ can be Taylor expanded close to the root

$$\vec{f}(\vec{x}_{n+1}) \approx \vec{f}(\vec{x}_n) + J_f(\vec{x}_n)(\vec{x}_{n+1} - \vec{x}_n). \tag{1.41}$$

Here, $J_f(\vec{x})$ is the Jacobian matrix of $\vec{f}(\vec{x})$ and $\vec{x}_n$ is the $\vec{x}$-value of the n-th step. To find the root, $\vec{f}(\vec{x}_{n+1})$ is replaced by 0 and with $\Delta\vec{x} = \vec{x}_{n+1} - \vec{x}_n$ it follows that

$$J_f(\vec{x}_n)\Delta\vec{x} = -\vec{f}(\vec{x}_n) \tag{1.42}$$

where $\vec{x}_{n+1} = \vec{x}_n + \Delta\vec{x}$. This system can be numerically solved by an Gaussian algorithm. If the L2-norm of $\Delta\vec{x}$ becomes smaller than the tolerance δ the algorithm is terminated.

By using this method, a simple parameter continuation of $\vec{G}(\vec{x}, \lambda) = 0$ in dependence of λ can be made. Therefore after finding the first $(\vec{x}_j, \lambda_j)$ which solves $\vec{G}(\vec{x}_j, \lambda_j) = 0$ a new pair $(\vec{x}_{j+1}, \lambda_{j+1})$ with $\lambda_1 = \lambda_0 + \Delta\lambda$ which solves the same equation should be found. Therefore, the tangent of $\vec{x}(\lambda)$ at $(\vec{x}_j, \lambda_j)$ is used to predict the starting value $\vec{x}_{j+1}^{(0)}$. This value is plugged into the Newton method to find the solution of $\vec{G}(\vec{x}_{j+1}, \lambda_{j+1}) = 0$.

To derive the tangent $\frac{\partial\vec{x}}{\partial\lambda}$, the equation $\vec{G}(\vec{x}, \lambda) = 0$ has to be differentiated

$$J_G(\vec{x}, \lambda)\frac{\partial\vec{x}}{\partial\lambda} + \frac{\partial\vec{G}(\vec{x}, \lambda)}{\partial\lambda} = 0 \tag{1.43}$$

So, to compute the tangent a problem similar to Eq. (1.42) has to be solved

$$J_G(\vec{x}, \lambda)\frac{\partial\vec{x}}{\partial\lambda} = -\frac{\partial\vec{G}(\vec{x}, \lambda)}{\partial\lambda} \tag{1.44}$$

This method works well if there is one-to-one correspondence of the solution $\vec{x}$ and the parameter λ, but breaks down at saddle-node bifurcations. To fix this, the parameter λ and the solution vector $\vec{x}$ can be combined into a new solution vector $\vec{y} = (\vec{x}, \lambda)$ written as function of a new control parameter s.

The parameter s is defined as the arclength of the curve $\vec{x}(\lambda)$. The local approximation

$$|\Delta\vec{x}|^2 + (\Delta\lambda)^2 = (\Delta s)^2 \tag{1.45}$$

is used to obtain an additional equation $p(\vec{x}, \lambda, s) = 0$ that shall complement G. With

$$|\Delta\vec{x}|^2 = (\vec{x}_{j+1} - \vec{x}_j)\frac{(\vec{x}_{j+1} - \vec{x}_j)}{\Delta s}\Delta s \approx (\vec{x}_{j+1} - \vec{x}_j)\frac{\partial\vec{x}}{\partial s}\Delta s \tag{1.46}$$

and

$$(\Delta\lambda)^2 \approx (\lambda_{j+1} - \lambda_j)\frac{\partial\lambda}{\partial s}\Delta s \tag{1.47}$$

it follows for $p(\vec{x}, \lambda, s)$

$$p(\vec{x}, \lambda, s) = (\vec{x}_{j+1} - \vec{x}_j)\frac{\partial\vec{x}}{\partial s} + (\lambda_{j+1} - \lambda_j)\frac{\partial\lambda}{\partial s} - \Delta s \tag{1.48}$$

With this equation a new system of equations is introduced by defining

$$\vec{E}(\vec{y}, s) = \begin{pmatrix} \vec{G}(\vec{x}, \lambda) \\ p(\vec{x}, \lambda, s) \end{pmatrix} = 0 \tag{1.49}$$

With the new Jacobian of $\vec{E}$ (J_E) the same algorithm can be used to continue the new system. Because the arclength is a variable which grows with every continuation step, this algorithm does not break down at saddle-node bifurcation.

1.5.1 Detection of bifurcation points and switching branches

One property of a fixed point of a differential equation is its stability. If a fixed point is linearly stable any infinitely small perturbation $\delta\vec{v}$ about the fixed point $\vec{x_0}$ decays if the time is progressing ($t \to \infty$). If there exists a perturbation $\delta\vec{w}$, which grows with time, the fixed point is unstable.

To make a more quantitative statement, we Taylor-expand the differential equation close to the fixed point $\vec{x}_0$:

$$\partial_t\psi(\vec{x}_0 + \delta\vec{v}) \approx \vec{G}(\vec{x}_0, \lambda) + J_G(\vec{x}_0, \lambda)\delta\vec{v} = J_G(\vec{x}_0, \lambda)\delta\vec{v}. \tag{1.50}$$

It follows, that a fixed point is linearly stable precisely when the Jacobian matrix $J_G(\vec{x}_0, \lambda)$ at the fixed point is negative definite. It follows that all eigenvalues of the Jacobian should have a negative real part. If the Jacobian has a positive eigenvalue (positive real part of the eigenvalue), perturbation which are linearly dependent on the corresponding eigenvector grow for $t \to \infty$.

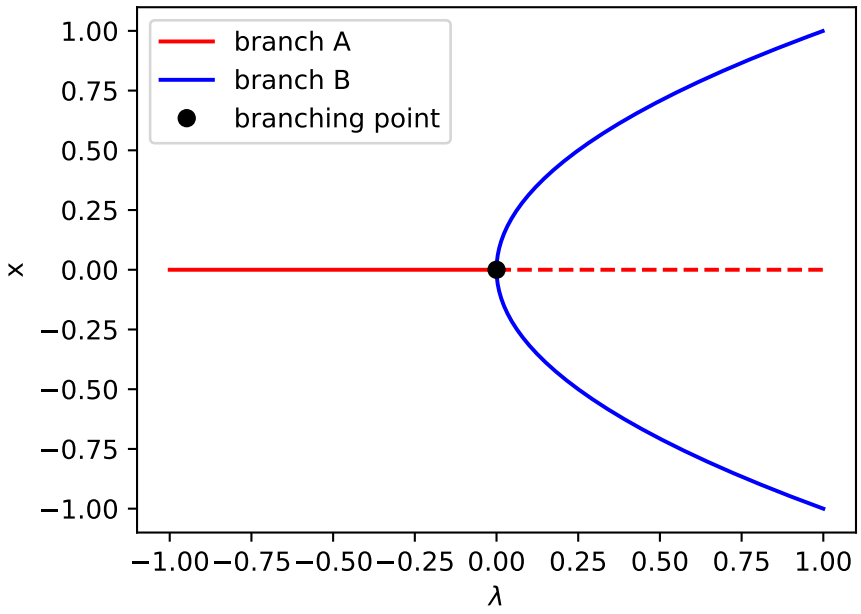

Figure 1.1: Example of a pitchfork bifurcation in 1D. The solid lines are the stable fixed points and the doted line is the unstable solution.

Changes of the stability encountered in a continuation process with respect to a parameter λ can have two reasons. The first reason is a change of the sign of $\Delta\lambda = \lambda_{n+1} - \lambda_n$ between two steps at fold points. The second reason are branching points. At branching points two different solution branches cross each other.

A special case are pitchfork bifurcations (Fig. 1.1). For pitchfork bifurcation follows for one branch (in Fig. 1.1 branch B), that after crossing the branch point the number of positive eigenvalues does not change, but at the branch point one eigenvalue is equal to zero. In this case only the sign of $\Delta\lambda$ change. So to detect branch points it will be looked on the number of positive eigenvalues and on the sign of $\Delta\lambda$.

To find the direction of the crossing solution branch, it will be assumed, that we follow the branch A and branch B cross branch A (see Fig. 1.1) . At the branch point the Jacobian J_G of branch A has an eigenvalue, which is equal to zero. The corresponding eigenvector is the tangent of branch B. So to switch to branch B the branch point will be chosen as starting point and the eigenvector is the starting direction.

1.5.2 Finding binodal modes

Additionally to bifurcation diagrams also the existence of binodal modes can be used to analyze non-linear models. Binodals are to different stable states which can coexist at the same temperature T and chemical potential μ. For them follows, that they does not apply pressure on each other.

A system with binodals is the conserved Swift Hohenberg model [9]:

$$\Omega = \int \mathrm{d}x \, \frac{\varphi^4}{4} + \frac{\varphi}{2}\left(r + (k_{\text{crit}}^2 + \partial_x^2)^2\right)\varphi - \mu\varphi(x) \tag{1.51}$$

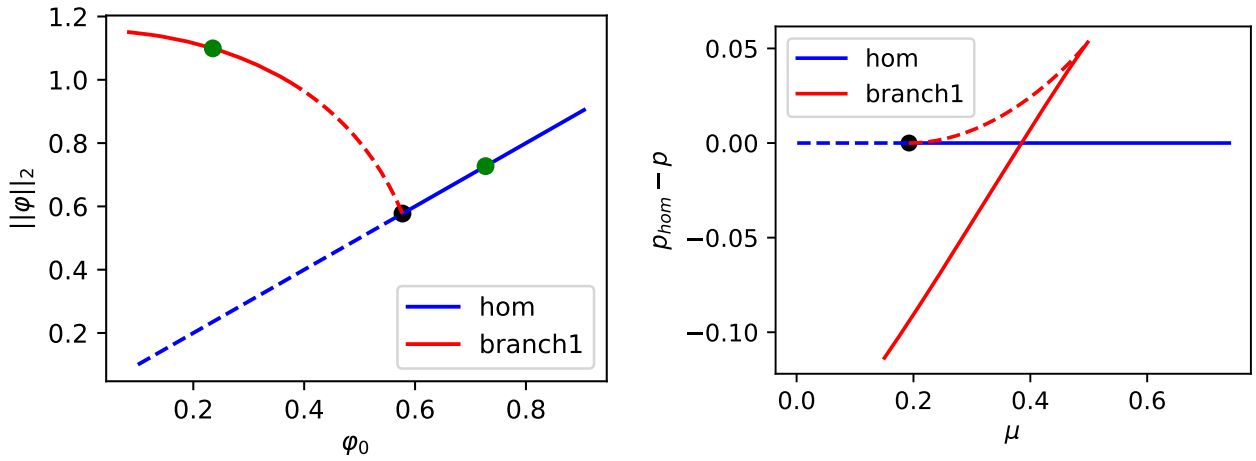

Figure 1.2: Bifurcation diagrams for $r = -1$. The black points are the bifurcation points. The green points of the left picture are the mean densities of the two binodals.

r is a temperature constant. As general $\Omega = -pV$. In this case $k_{\text{crit}} = 1$. Now it will be searched for a special μ and temperature r a crystalline state which has the same pressure p as a homogeneous state with the same global influences (Fig. 1.2). This state should solve the DFT equation (1.7).

First, the continuation algorithm should be run with a homogeneous state as initial condition with μ as continuation parameter. Here the branch points should be found and the stable region of this solution should be big enough. Then it will be switched on the other fixed states. If during the continuation of these state the $p(\mu)$ curve cross the $p_{\text{hom}}(\mu)$ curve of the uniform solution, the binodals for a given r are found. During the contiuation steps of the branch of the crystalline state it can be helpful to compute also the density of the uniform solution, which solves the DFT-equation (1.7) with the same chemical potential μ and the same variable r. This variable can be used to compute the pressure difference between the liquid and the crystalline state directly.

Additionally to the derivation of the binodals, it can be seen in figure 1.2 what happens if the roll of a free parameter and the continuation parameter changes. Because the roll of a parameter does not change the equation system $\vec{G}(\vec{x}, \lambda) = 0$ the trajectory of the branch does not differ. In this case the free parameter would be a part of $\vec{x}$ and the continuation parameter remains λ. But a change of the roll of the parameter would change the Jacobian matrix. So also the number of his positive eigenvalues can be changed. As it can be seen in the left diagram of figure 1.2 the pitchfork bifurcation is supercritical if the algorithm will be run with φ_0 as the continuation parameter. In this case the entire branch 1 is stable. But in the shown case with μ as continuation parameter the bifurcation is subcritical and branch 1 is unstable until the fold bifurcation. In this thesis, opened systems will be discussed. So during continuation parameter which depend on the temperature or the chemical potential are fixed or will be used as continuation parameter.

If the binodals of one r_0 is found, the dependences of the binodals with respect to r can be derived. Therefor a new continuation with r as continuation parameter will be started. The previously founded binodals at r_0 are the initial conditions. During the continuation, the pressure difference $p_{\text{hom}} - p$ will be fixed on zero. In this case the solution is shown in figure 1.3. By changing the sign of μ and φ it can be shown, that we get the same equations for the pressure p and the DFT equation 1.7. The model and the corresponding phase diagrams are inversion invariant. It follows that the binodals of Ref. [9] are equal to the derived binodals of figure 1.3.

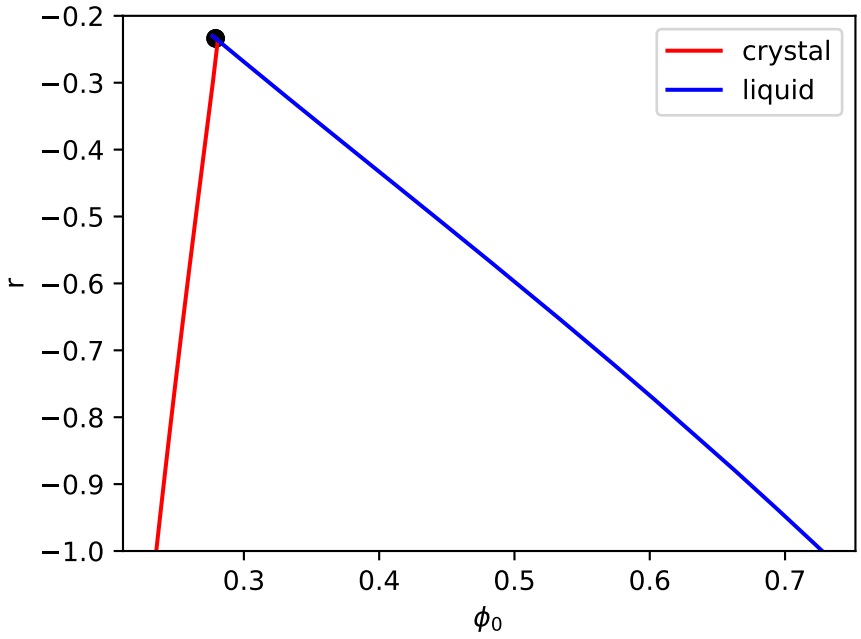

Figure 1.3: The two binodals of the Swift Hohenberg model

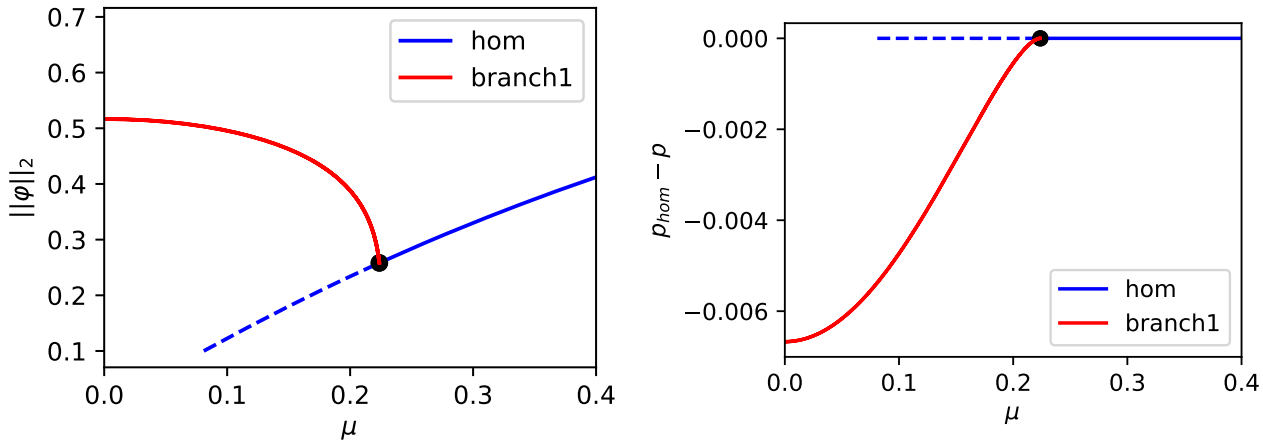

Figure 1.4: Bifurcation diagrams for $r = -0.2$. The black points are the bifurcation points. The Swift Hohenberg model has no binodals for $r = -0.2$.

As it can be seen in figure 1.3 the Swift Hohenberg model has none binodals for $r > -\frac{9}{38}$ [9, 10]. But the uniform solution has unstable regions if $r < 0$. So the algorithm will be run with an r which is smaller then zero and bigger then the tricritical point $r = -\frac{9}{38}$. As it can seen in figure 1.4, that now the pitchfork bifurcation is supercritical. So the $p(\mu)$ diagrams of the two different branch can not cross each other. It follows, if the continuation will be run with μ (or a temperature dependent parameter) as continuation parameter, and the bifurcations from a stable solution is supercritical, the system have none binodal.

2 The GEM4 PFC Model

Next we consider a model for soft particles, that have an attractive potential of the form [11]

$$\mathcal{F}_{\text{exc}} = \int_{-\infty}^{\infty} \mathrm{d}x \int_{-\infty}^{\infty} \mathrm{d}x' \frac{\alpha}{2} \exp\left(- \left(\frac{x - x'}{R} \right)^4 \right) \rho(x)\rho(x') \tag{2.1}$$

This model will be discussed in the 1d and the 2d case.

2.1 The PFC Model in 1d

First of all, a correlation function $c(x)$ has to be derived. Here, only the two-particle correlation function is different from zero. With equation (1.14) this correlation function has the form

$$c(x) = c^{(2)}(x) = -\beta\alpha \exp\left(- \left(\frac{x}{R} \right)^4 \right). \tag{2.2}$$

In the next step the moments $\tilde{A}^{(2)}_{2\mu,r}$ are computed (table 1.1). We obtain

$$\begin{aligned} \tilde{A}^{(2)}_{2\mu,r} &= -\frac{2}{(2\mu)!}\alpha\beta \int_0^{\infty} \mathrm{d}r\, r^{2\mu} \exp\left(- \left(\frac{r}{R} \right)^4 \right) = -\frac{2}{(2\mu)!}\alpha\beta \int_0^{\infty} \mathrm{d}u\, u^{2\mu} R^{2\mu+1} \exp\left(- u^4 \right) \\ &\overset{u=v^{1/4}}{=} -\frac{\alpha\beta}{(2\mu)!2} R^{2\mu+1} \int_0^{\infty} \mathrm{d}v\, v^{\frac{2\mu-3}{4}} \exp\left(-v\right) = -\frac{\alpha\beta}{(2\mu)!2} R^{2\mu+1} \Gamma\left(\frac{2\mu+1}{4} \right). \end{aligned} \tag{2.3}$$

As a result, the PFC equation (1.29) (for $U_{\text{ext}} = 0$) has the form

$$\partial_t \psi = D_T \partial_x \left[(1+\psi) \partial_x \left(- k_{\text{B}} T \sum_{n=1}^{2M+1} \frac{(-\psi)^n}{n} + \rho_{\text{ref}} \frac{\alpha R}{2} \sum_{\mu=0}^{M} \frac{R^{2\mu}}{(2\mu)!} \Gamma\left(\frac{2\mu+1}{4} \right) \partial_x^{2\mu} \psi \right) \right]. \tag{2.4}$$

Here $M = \frac{N}{2}$. With $x = \tilde{x}R$, $\eta = \rho_{\text{ref}} \frac{\alpha R}{2 k_{\text{B}} T}$ and $\tilde{t} = \frac{D_T k_{\text{B}} T}{R^2} t$ this equation can be rewritten in the nondimensional form (dropping the tilde):

$$\partial_t \psi = \partial_x \left[(1+\psi) \partial_x \left(- \sum_{n=1}^{2M+1} \frac{(-\psi)^n}{n} + \eta \sum_{\mu=0}^{M} \frac{1}{(2\mu)!} \Gamma\left(\frac{2\mu+1}{4}\right) \partial_x^{2\mu} \psi \right) \right] \tag{2.5}$$

Without the expansion of the ideal part (i.e. PFC equation (1.40)) the scaled specific PFC equation for the GEM4 model has the form

$$\partial_t \psi = \partial_x^2 \psi + \eta \partial_x \left[(1+\psi) \partial_x \left(\sum_{\mu=0}^{M} \frac{1}{(2\mu)!} \Gamma\left(\frac{2\mu+1}{4}\right) \partial_x^{2\mu} \psi \right) \right] \tag{2.6}$$

2.2 Linear stability analysis of the PFC model

One of the fixed points (uniform solutions) of equation (2.5) is the homogeneous state $\psi(x) = \psi_0$ of abitrary ψ_0. To analyze the linear stability of the homogeneous state, we use the ansatz

$$\psi(x,t) - \psi_0 = \varepsilon \exp\left(\lambda t - ikx\right) \tag{2.7}$$

with $\varepsilon \ll 1$ and introduce it into the partial differential equation (2.5). To order $\mathcal{O}(\epsilon)$ we find

$$\lambda_1^{(2M)} = -k^2(1+\psi_0)\left[\tilde{\lambda}_{\mathsf{id},2M} - \tilde{c}_{2M}(k)\right] = -k^2(1+\psi_0)\left[\sum_{n=0}^{2M}(-\psi_0)^n + \eta \sum_{\mu=0}^{M} \frac{(-k^2)^\mu}{(2\mu)!}\Gamma\left(\frac{2\mu+1}{4}\right)\right] \tag{2.8}$$

$\tilde{c}_N(k)$ is the scaled Fourier transformed correlation function and $\lambda_{\mathsf{id},N} = k^2 \tilde{\lambda}_{\mathsf{id},N}$ is the ideal part of the dispersion relation. This function and the correlation function of the 8th, 12th and 16th order model are shown in figure 2.1.

If M is an odd number, the summand of highest order in k is positive. It follows for odd M, that $\lambda \to \infty$ if $k \to \infty$. Because this is unphysical, only systems where 4 is a divisor of N will be examined.

If $M \to \infty$ it follows

$$\sum_{n=0}^{\infty}(-\psi_0)^n = \frac{1}{1+\psi_0}$$

$$\begin{aligned}\sum_{\mu=0}^{\infty} \frac{k^{4\mu}}{(4\mu)!}\Gamma\left(\frac{4\mu+1}{4}\right) &= \Gamma\left(\frac{1}{4}\right)\left[1 + \sum_{\mu=1}^{\infty}\left(\frac{k^4}{4}\right)^\mu \prod_{n=1}^{\mu} \frac{4n-3}{4n(4n-1)(4n-2)(4n-3)}\right] \\ &= \Gamma\left(\frac{1}{4}\right) {}_0F_2\left(;\frac{1}{2},\frac{3}{4};\frac{k^4}{256}\right)\end{aligned}$$

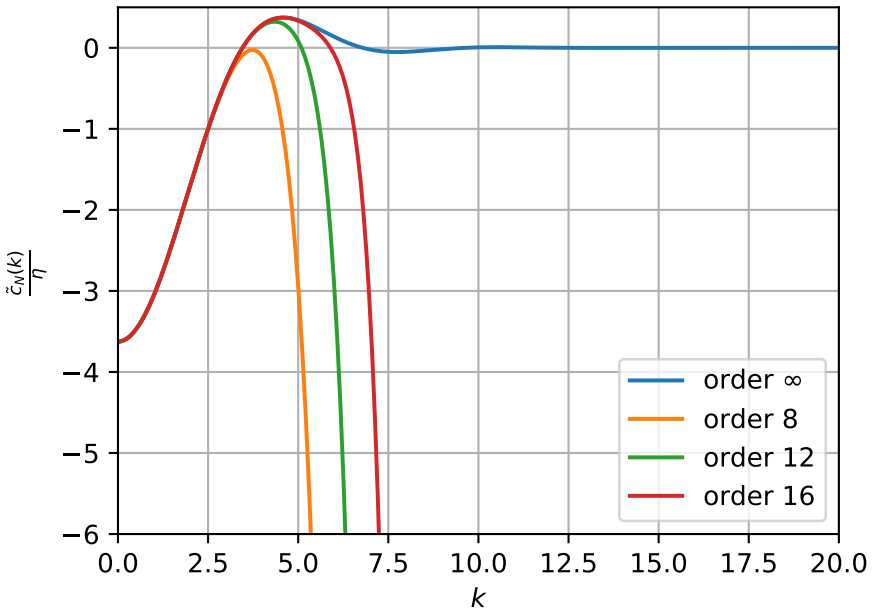

Figure 2.1: Fourier transformed correlation function of the GEM4 model to different order of approximation as given in the legend. $N = \infty$ stands for the exact DFT model. Expanded about $k = 0$.

$$\sum_{\mu=0}^{\infty} \frac{k^{4\mu+2}}{(4\mu+2)!}\Gamma\left(\frac{4\mu+3}{4}\right) = \Gamma\left(\frac{3}{4}\right)\frac{k^2}{2}\left[1+\sum_{\mu=1}^{\infty}\left(\frac{k^4}{4}\right)^{\mu}\prod_{n=1}^{\mu}\frac{4n-1}{(4n+2)(4n+1)4n(4n-1)}\right]$$
$$= \frac{k^2}{2}\Gamma\left(\frac{3}{4}\right){}_0F_2\left(;\frac{3}{2},\frac{5}{4};\frac{k^4}{256}\right)$$

Where the ${}_pF_q$ are the hypergeometric functions

$${}_pF_q(a_1,...,a_i,...,a_p;b_1,...,b_j,...,b_q;z) = \sum_{n=0}^{\infty}\frac{\prod_{i=1}^{p}(a_i)_n}{\prod_{j=1}^{q}(b_j)_n}\left(\frac{z^n}{n!}\right) \tag{2.9}$$

with the Pochhammer symbols

$$(x)_n = \frac{\Gamma(x+n)}{\Gamma(x)} \tag{2.10}$$

If p or q is 0, the product over a_i or b_j is replaced by 1.

All in all the dispersion relation with $M \to \infty$ has the form

$$\lambda^{(\infty)} = -k^2 - k^2(1+\psi_0)\frac{\eta}{2}\left[2\Gamma\left(\frac{1}{4}\right){}_0F_2\left(;\frac{1}{2},\frac{3}{4};\frac{k^4}{256}\right) - k^2\Gamma\left(\frac{3}{4}\right){}_0F_2\left(;\frac{5}{4},\frac{3}{2};\frac{k^4}{256}\right)\right] \tag{2.11}$$

The global maximum of the 8th order correlation function is slightly smaller than 0 (see figure 2.1). This holds for any η. Because $\tilde{\lambda}_{\mathsf{id},N}$ for even N is always larger than 0, the uniform solution of the 8th order model is always stable. Therefore, here only higher order models are discussed.

The correlation function of the order ∞ model has a global maximum at $k_{\mathsf{max},\infty} = 4.59$ with $\tilde{c}(k_{\mathsf{max}})/\eta = 0.375$. The difference of $k_{\mathsf{max},\infty}$ and $k_{\mathsf{max},16}$ for order $N = 16$ is still nearly 0.01 and for $N = 12$ it is nearly 0.25. The difference between $\tilde{c}(k_{\mathsf{max},\infty})/\eta$ and $\tilde{c}_{16}(k_{\mathsf{max},16})/\eta$ is 0.002 and for $\tilde{c}_{12}(k_{\mathsf{max},12})/\eta$ it is 0.05. It can be shown, that the maximum of $\tilde{c}(k)$ defines the spinodal of the system and the position k is the wavenumber of the new stable state.

Next the dispersion relation of the exact and the 12th and the 16th order model are discussed. In figure 2.2 also the dispersion relations $\lambda_2^{(N)}$ of the models with the exact ideal term are shown. They have the form

$$\lambda_2^{(2M)} = -k^2\left[1 + (1+\psi_0)\eta\sum_{\mu=0}^{M}\frac{(-k^2)^\mu}{(2\mu)!}\Gamma\left(\frac{2\mu+1}{4}\right)\right] = -k^2\left[1 - (1+\psi_0)\tilde{c}_{2M}(k)\right] \tag{2.12}$$

Because $\tilde{\lambda}_{\mathsf{id},\infty}$ is a series that does not converge for $\psi_0 \geq 1$, the difference between the dispersion relation $\lambda_1^{(N)}(k)$ and $\lambda^{(\infty)}$ become even lager for increasing order N and $\psi_0 > 1$. Also, the PFC equation becomes simpler when the ideal part is not expand. So the following discussion only considers PFC equations of type 2.

2.2.1 The spinodal of the GEM4 model

The homogeneous state becomes linearly unstable if the dispersion relation is positive for a range of wavenumbers k. With equation (2.12) this is the case for

$$1 < (1+\psi_0)\tilde{c}_N(k) \tag{2.13}$$

With the Fourier transformed correlation function of the GEM4 model (see (2.12)) this relation can be reformulated as

$$\frac{1}{\eta} < -(1+\psi_0)\sum_{\mu=0}^{M}\frac{(-k^2)^\mu}{(2\mu)!}\Gamma\left(\frac{2\mu+1}{4}\right) \tag{2.14}$$

It follows that the spinodal is linear with the maximum of $\frac{\tilde{c}_N}{\eta}$ as the gradient (see figure 2.3).

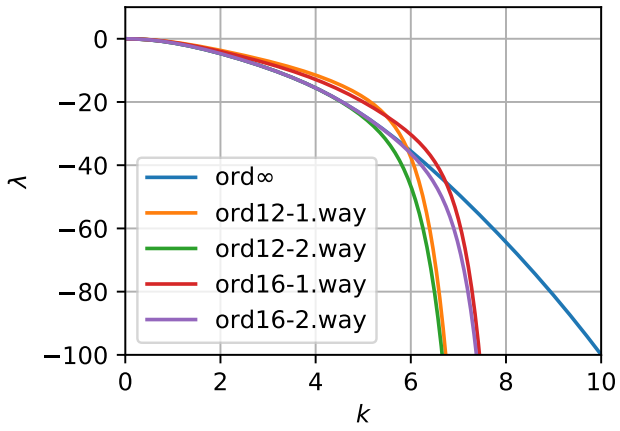

(a) $\psi_0 = -0.9, \eta = 1$

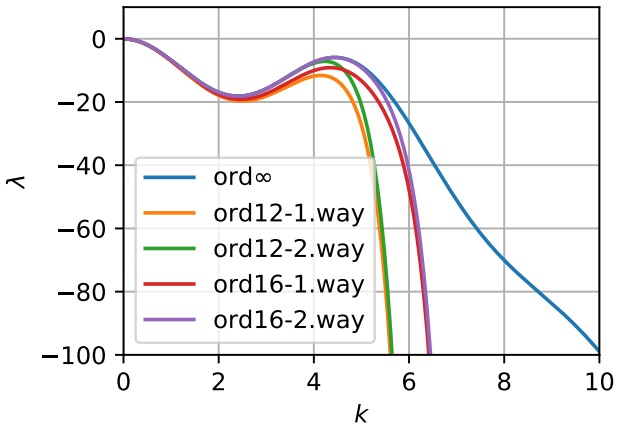

(b) $\psi_0 = 0.9, \eta = 1$

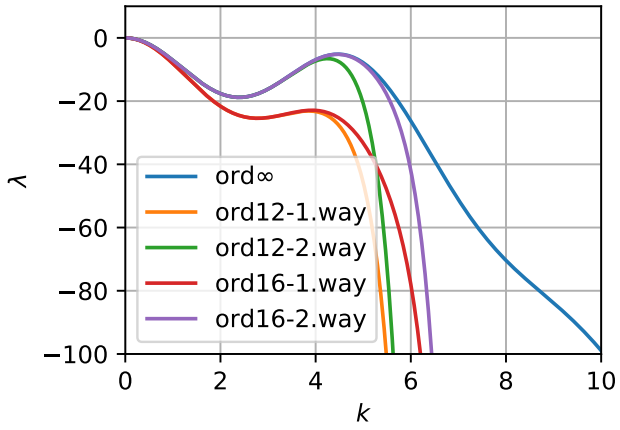

(c) $\psi_0 = 1, \eta = 1$

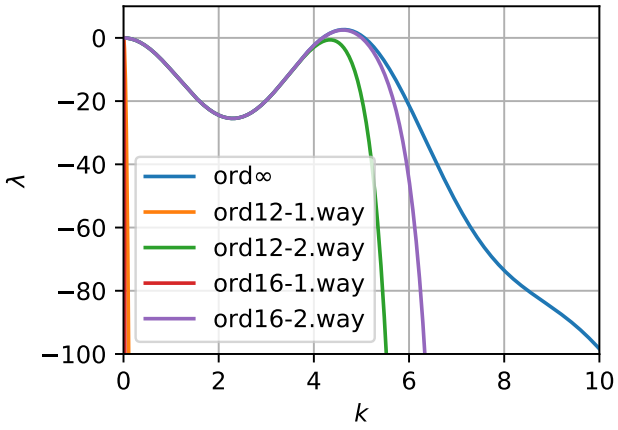

(d) $\psi_0 = 2, \eta = 1$

Figure 2.2: Dispersion relation of the uniform solution of the GEM4 model. Expanded about $k = 0$

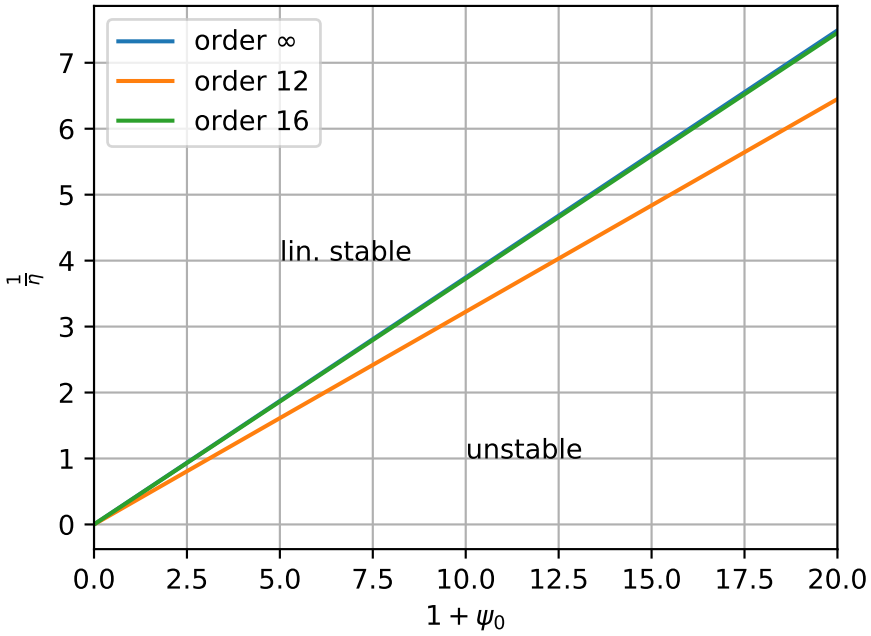

Figure 2.3: Linear stability diagram of the GEM4 model. From here onwards only type 2 PFC models are used.

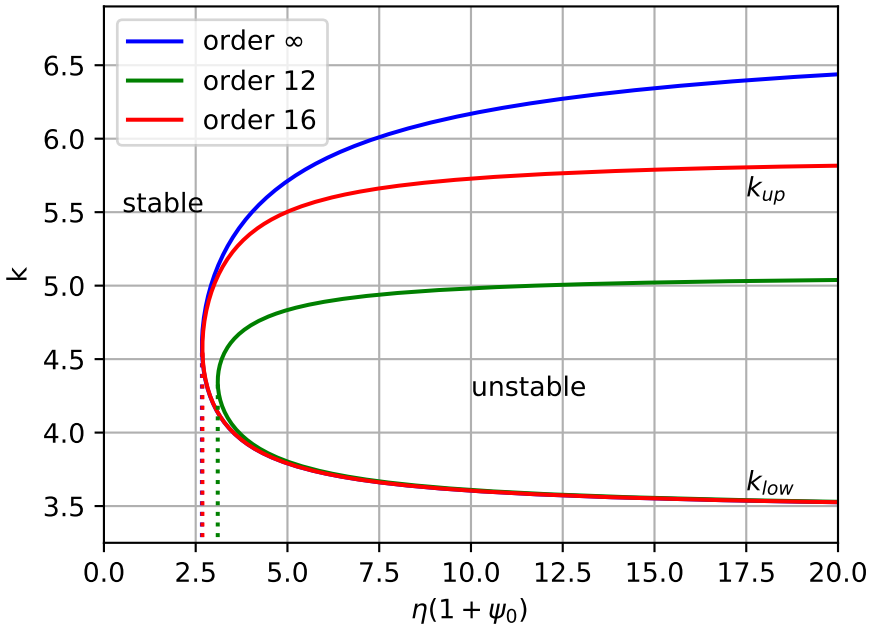

Figure 2.4: Linear stability of the uniform solution of the PFC models obtained by expansion about $k = 0$ from GEM4 DDFT ($N = \infty$). The state is unstable for k between the upper and the lower limit, k_{up} and k_{low}. The vertical dotted lines are the inverse of the maxima values $\tilde{c}_N(k_{\max,N})$. $\tilde{c}_N(k_{\max}, N)$ are also slope of the spinodals in figure 2.3.

The relation (2.14) can also be used to determine the unstable k range. Division by $(1+\psi_0)$ and inversion gives

$$\eta(1+\psi_0) > -\frac{1}{\sum_{\mu=0}^{M} \frac{(-k^2)^\mu}{(2\mu)!}\Gamma\left(\frac{2\mu+1}{4}\right)} = \frac{\eta}{\tilde{c}_N(k)} \tag{2.15}$$

To find the border of the unstable k space with respect to $\eta(1+\psi_0)$, a k between the zero points around the global maximum of the Fourier transformed correlation function has to be plugged into Eq. (2.15). As can be seen in figure 2.4, the homogeneous state for $\eta(1+\psi_0) > \frac{\eta}{\tilde{c}_N(k_{\mathsf{max},N})}$ is unstable for k if this k lays between the upper limit k_{up} and the lower limit k_{low}.

The lower limit is for all GEM4 models nearly identical. But the systems of lower order have a smaller upper limit. As noted before, also k_{max}, the wavelength of the periodic mode, which destabilize the uniform solution, becomes smaller, if the order N decreases.

2.3 A new gradient expansion of the GEM4 model

As seen in the previous section, the Fourier transformed correlation functions of the approximated PFC models do not converge fast. So a model of 12th order is needed to get a system with a spinodal and a model of 16th order to get a system with an spinodal which closely follows the one of the DFT model ($N=\infty$). To improve the convergence of the correlation function, the gradient expansion can be done centred about its maximum. In this case, the Fourier transformed correlation function is expanded in k^2 around k^2_{max}:

$$\tilde{c}_M(k) = \eta \sum_{m=0}^{M} \frac{B_m}{m!}(k^2 - k^2_{\mathsf{max}})^m \tag{2.16}$$

Here $2M$ is the order of the PFC equation. After the back-transformation of the correlation function, the new PFC equation has the form:

$$\partial_t \psi = \partial_x^2 \psi - \partial_x(1+\psi)\partial_x \eta \sum_{m=0}^{M} \frac{B_m}{m!}(-\partial_x^2 - k^2_{\mathsf{max}})^m \psi \tag{2.17}$$

Here, the moments B_m are:

$$B_{2u} = -\frac{1}{4^{3u}}\left[\frac{\Gamma(\frac{3}{4})\Gamma(\frac{1}{4})}{\Gamma(\frac{3}{4}+u)}{}_0F_2\left(;\frac{1}{2},\frac{3}{4}+u;\frac{k^4_{\mathsf{max}}}{256}\right) - \frac{k^2_{\mathsf{max}}}{2}\frac{\Gamma(\frac{3}{4})\Gamma(\frac{5}{4})}{\Gamma(\frac{5}{4}+u)}{}_0F_2\left(;\frac{3}{2},\frac{5}{4}+u;\frac{k^4_{\mathsf{max}}}{256}\right)\right] \tag{2.18a}$$

$$B_{2u+1} = -\frac{1}{4^{3u}}\left[\frac{k^2_{\mathsf{max}}}{4^3}\frac{\Gamma(\frac{3}{4})\Gamma(\frac{1}{4})}{\Gamma(\frac{7}{4}+u)}{}_0F_2\left(;\frac{3}{2},\frac{7}{4}+u;\frac{k^4_{\mathsf{max}}}{256}\right) - \frac{1}{2}\frac{\Gamma(\frac{3}{4})\Gamma(\frac{5}{4})}{\Gamma(\frac{5}{4}+u)}{}_0F_2\left(;\frac{1}{2},\frac{5}{4}+u;\frac{k^4_{\mathsf{max}}}{256}\right)\right] \tag{2.18b}$$

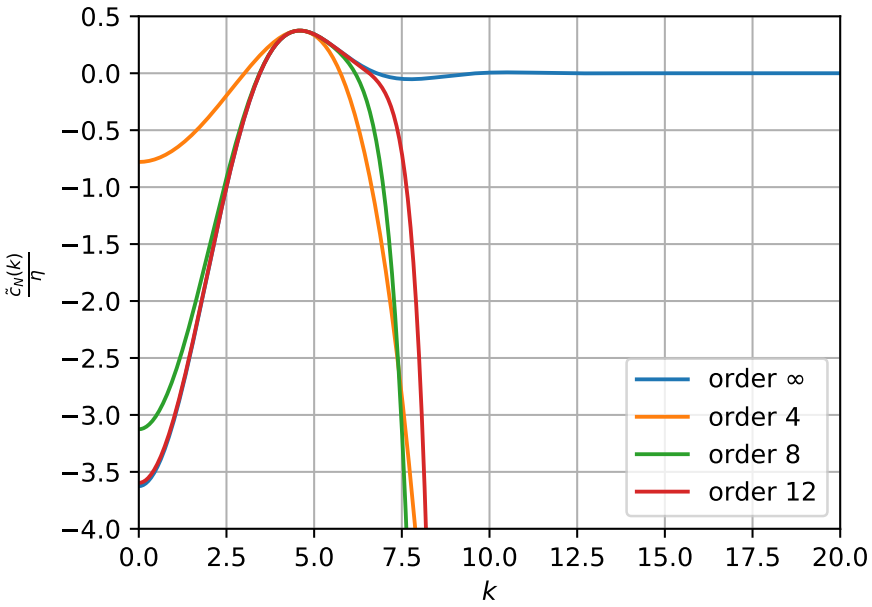

Figure 2.5: Fourier transformed correlation function of the new PFC GEM4 model. Expanded about $k = k_{\text{max}}$

.

and u is a non-negative integer. It can be shown, that all moments B_m with odd m are positive and all moments with even $m \neq 0$ are negative. So, similar to the PFC equation (2.6), only systems where 4 is a divisor of the order $N = 2M$ are physically reasonable.

Figure 2.5 shows correlation functions of the new expanded models. By definition, the global maxima of all correlation functions of different order are always at $k = k_{\text{max}}$ and have always the same height. So it follows, that the uniform solution of all systems becomes unstable at the same parameter value with respect to a periodic state of the same wavenumber k_{max}.

However, the lower and upper border of the unstable $k-$region of the 4th order model are both at smaller k values than for the exact model (see figure 2.6). By increasing the order N, this difference decreases. For instance, the instability borders of the new 8th order model are more exact than the borders of the 16th order model with the gradient expansion about $k = 0$.

However, the present set of models is less exact in the compressibility i.e. in the behavior at $k = 0$. The isothermal compressibility κ is defined in Ref. [2] by

$$1 - \tilde{c}_N(0) = \frac{\rho_{\text{ref}} k_B T}{\kappa} \tag{2.19}$$

The different will be caused by the differences between $\tilde{c}_\infty(0)$ and $\tilde{c}_N(0)$. But by comparing figure 2.1 and 2.5 it can be seen, that these differences decrease faster with increasing order in expansion than the differences between the positions of the maxima of $\tilde{c}_\infty$ and $\tilde{c}_N$ of the previous models that were expanded about $k = 0$. These differences are shown in tables 2.1 (left) and 2.1 (right)

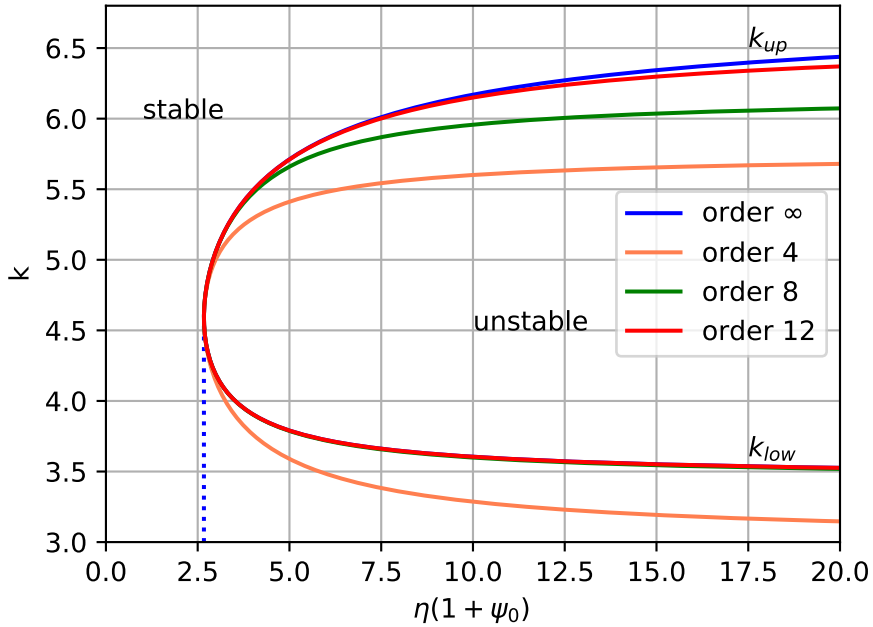

Figure 2.6: Linear stability of the uniform solution of the PFC models obtained by expansion about $k = k_{\max}$ from GEM4 DDFT ($N = \infty$). The state is unstable for k between the upper and the lower limit, k_{up} and k_{low}. The vertical dotted line is the inverse of the maximum value $\tilde{c}_N(k_{\max})$. $\tilde{c}_N(k_{\max})$ is also slope of the spinodal of the model of order ∞ in figure 2.3.

N	$k_{\max,N}$	$\tilde{c}_N(k_{\max,N})/\eta$
∞	4.59	0.375
12	4.35	0.322
16	4.58	0.373

N	$-\tilde{c}_N(k_{0,N})/\eta$
∞	3.626
4	0.779
8	3.126
12	3.625

Table 2.1: Quantitative comparison of the Fourier-transformed correlation functions of the full GEM4 model DDFT ($N = \infty$) and the corresponding PFC models of various order N obtained through expansion about $k = 0$ (left) and $k = k_{max}$ (right).

2.4 Continuation of the PFC model

After the analysis of the dispersion relation of the PFC equation it is known, when the homogeneous state becomes unstable. In the next step, the new stable solution of the PFC equation is obtained. Also, these solutions should solve the steady PFC equation. Therefor the PFC-equation can be integrated over the space x. Than the following equation have to be divided by the viscosity $D_T(1+\psi)$ and integrated again over the space. The steady PFC equation can be also derived by inserting the gradient expanded exchange part in the DFT equation (1.7)

$$\ln\left(\rho(\vec{r})\right) - \rho_{\mathsf{ref}}(c*\psi)(\vec{r}) - \mu = 0 \tag{2.20}$$

with $\rho(\vec{r}) = \rho_{\mathsf{ref}}(1+\psi(\vec{r}))$. In the following computation it will be assumed, that $\rho_{\mathsf{ref}} = 1$.

Due to the logarithm of the density with the singularity of the logarithm at $\rho(\vec{r}) = 0$, this equation can cause numerical problems if the densities becomes too small at a position $\vec{r}$. So this function will be reformulated into the equivalent form

$$1 + \psi(\vec{r}) - e^{\mu}\exp\left((c*\psi)(\vec{r})\right) = 0 \tag{2.21}$$

This function will be solved in a system with the system length $L = \frac{4\pi}{k_{\mathsf{max}}}$ and Neumann boundary conditions. So all solution of this equation can be expressed by:

$$\psi(x) = \sum_{i=0}^{N} \psi_n \cos\left(\frac{k_{\mathsf{max}}}{4} n x\right) \tag{2.22}$$

with $N \to \infty$ and

$$\psi_n = \frac{1}{2L}\int_0^{2L} \psi(x)\cos\left(\frac{k_{\mathsf{max}}}{4} n x\right) \cdot \begin{cases} 1 & \text{if } n = 0 \\ 2 & \text{if } n > 0 \end{cases} \tag{2.23}$$

So ψ and the whole equation (2.21) can be transformed in a pseudo Fourier space and the convolution becomes

$$(c*\psi)(x) = \sum_{i=0}^{N} \tilde{c}\left(\frac{n k_{\mathsf{max}}}{4}\right)\psi_n \cos\left(\frac{k_{\mathsf{max}}}{4} n x\right) \tag{2.24}$$

and the rest of the equation has the form:

$$\delta_{n,0} + \psi_n - \frac{1}{2L}\int_0^{2L} e^{\mu}\exp\left((c*\psi)(x)\right)\cos\left(\frac{k_{\mathsf{max}}}{4} n x\right)(2-\delta_{n,0}) = 0 \tag{2.25}$$

This equation is solved by using an arclength continuation. Here a modified version of the matlab tool pde2path is used [12, 13]. This tool will be used in the OOPDE setup. Therefore the Jacobian of (2.25) has to be computed.

$$J_{n,m} = \delta_{n,m} - \frac{1}{2L}\int_0^{2L} e^{\mu}\tilde{c}\left(\frac{mk_{\mathsf{max}}}{4}\right)\exp\left((c*\psi)(x)\right)\cos\left(\frac{k_{\mathsf{max}}}{4}mx\right)\cos\left(\frac{k_{\mathsf{max}}}{4}nx\right)(2-\delta_{n,0}) \quad (2.26)$$

The in pde2path needed mass matrix will be replaced by an unit matrix.

Due to the two integration of the PFC equation, the sign of all eigenvalue of the Jacobian matrix change. This means, that the Jacobian of a stable state has to be positive definite.

2.4.1 The Bifurcation diagram of the DDFT model

First the bifurcation diagram of the DDFT equation will be computed. Therefore, we choose $\eta = 2.5$ as a constant. μ is the continuation parameter. The solutions are shown in figure 2.7.

The DDFT equation has two different non uniform solutions. The stable solution is a gaussian comb with a periodic length of 1.369. The second solution is unstable and is also a gaussian comb. The periodic length of the second solution is 1.095. All branch points are supercritical pitchfork bifurcations. It follows, that in contrast to the 2d model GEM4 the 1d model GEM4 has none binodals [11].

2.4.2 The Bifurcation diagram of the PFC models of order N

Next the solution of the PFC equation (2.5) will be computed. As before μ is the continuation parameter and $\eta = 2.5$. To compare the models better with each other, the bifurcation diagrams and solutions will be shown in one figure (Fig. 2.8).

As it can be seen in figure 2.8 (c) and (d) the non uniform solutions of the discussed PFC models (2.5) are cosine functions with a constant offset ψ_0. It seems to be, that in contrast to the DDFT model the approximated models can not stimulate higher Fourier modes. So as it can be seen in figure 2.8 (a) that the norm of the solution of the approximated models are much smaller as the norm of the solution of the DDFT equation ($N = \infty$). In figure 2.8 (b) it is also to see, that also the pressure difference is smaller if the order N is small .

At the continuation a system length $L = \frac{4\pi}{k_{\mathsf{max}}}$ is chosen. Here, k_{max} is the maximum of the correlation function of the discussed model. In table 2.1 it can be seen that this k_{max} of the 12th order model is smaller than the k_{max} of the DDFT model. So the periodic length of the stable solution is bigger than the periodic length of the DDFT model. The periodic length of the stable solution of the higher order models are equal to the periodic length of the DDFT model.

To get a system which has a second non uniform solution the order N must be $N \geq 20$. Otherwise the uniform solution does not become unstable for a periodic solution with the length of 1.095.

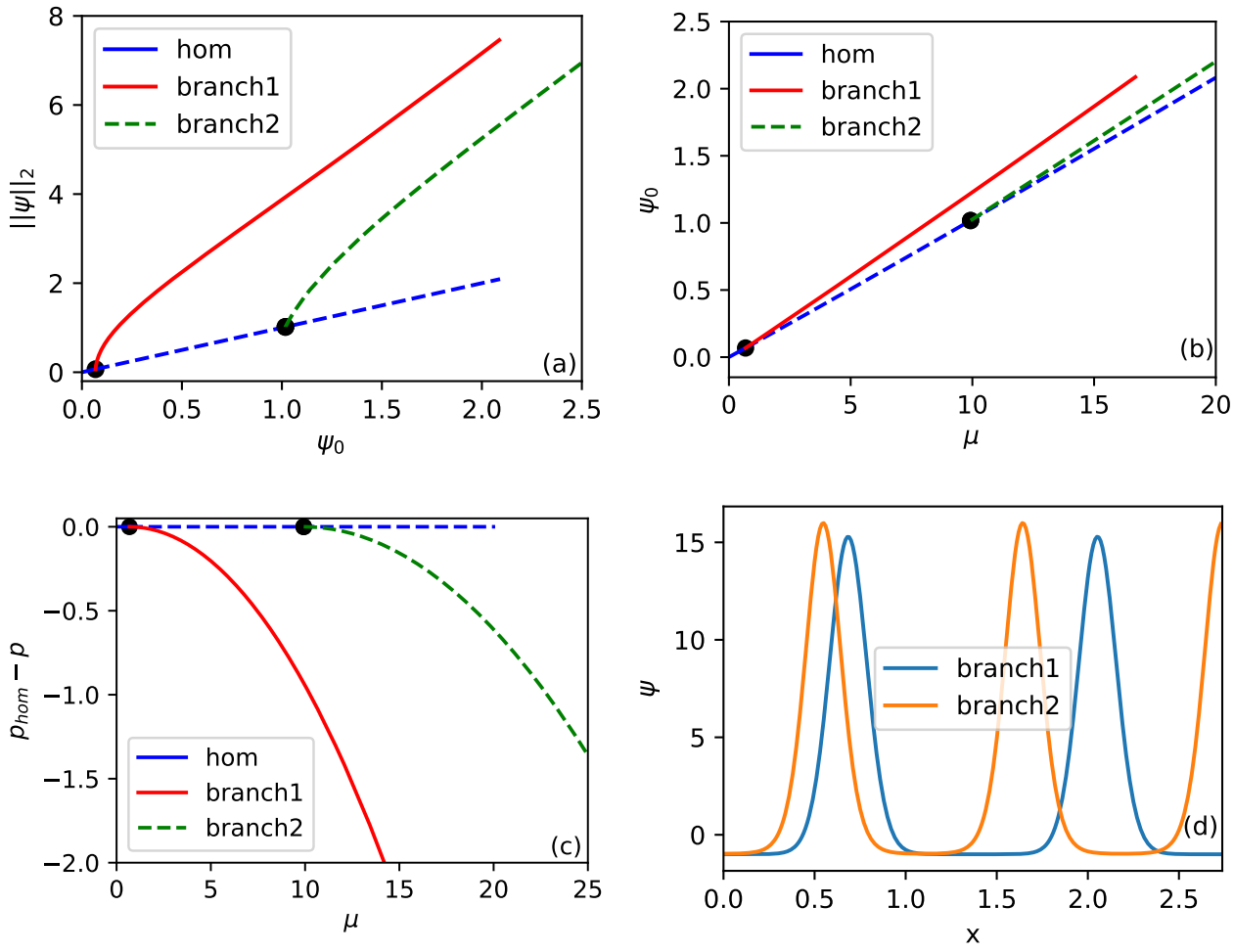

Figure 2.7: (a) Bifurcation diagram showing the norm of the solution of the DFT equation as function of ψ_0 with $\eta = 2.5$. (b) Dependence between ψ_0 from the chemical potential μ for each solution branch. (c) Pressure difference between the uniform solution and the derived solution. (d) The non uniform solution of the DFT equation.
The solution of branch 1 is stable, is a gaussian comb with an periodic length of 1.369. The printed solution solves the DFT equation with $\mu = 16.7$.The solution of branch 1 is unstable, is a gaussian comb with an periodic length of 1.095. The printed solution solves the DFT equation with $\mu = 25.9$.

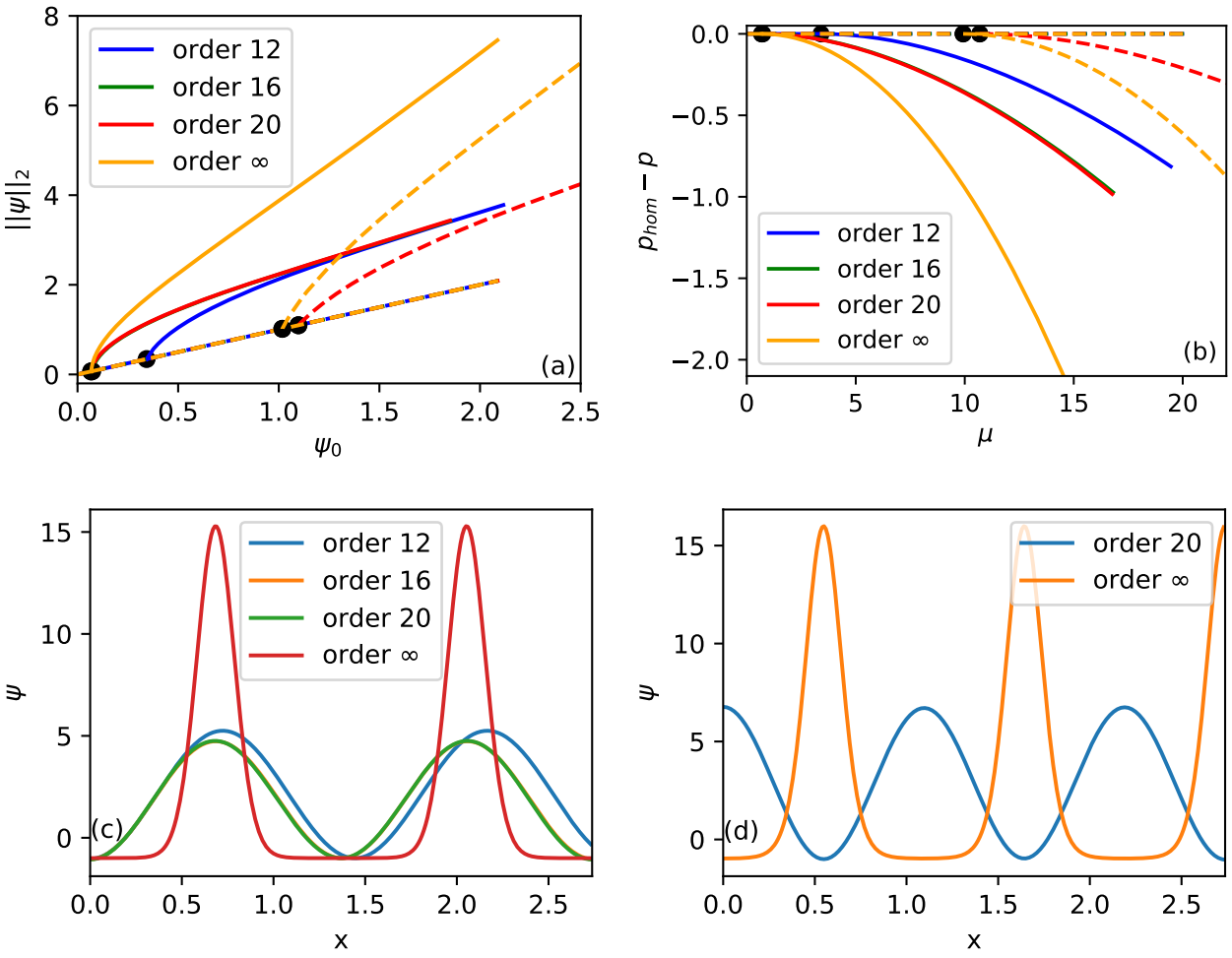

Figure 2.8: (a) Bifurcation diagram showing the norm of the solution of the PFC equation (2.5) as function of ψ_0 with $\eta = 2.5$. (b) Pressure difference between the uniform solution and the derived solution. (c) The solution of the PFC equation of branch 1. (d) The solution of the PFC equation of branch 2.
Here the stable solution of branch 1 of the PFC equation of low order is a cosine function with an periodic length of $\frac{2\pi}{k_{\max}}$ (see Tab. 2.1). The printed solution of 12th order has a chemical potential $\mu = 19.5$. The 16th and 20th order solution has a chemical potential of $\mu = 16.8$. To get a model, which has a second non uniform solution, the order N have to be $N \geq 20$. In this case the solution is a cosine function with a periodic length of 1.095 and has a chemical potential of $\mu = 26.8$.

The position of the bifurcation points changes in comparison to the DDFT models. The mean density $1 + \psi_0$ must be bigger to destabilize the uniform solution of the PFC models. Because the mean density grows with the chemical potential μ, the chemical potential must also become bigger to stimulate the periodic solutions. These differences decreases if the order N grows.

Finally the solutions of the model (2.6) will be analyzed. Here the role of μ and η does not change in comparison t0 the DDFT model.

In figure 2.9 (a) it is to see that the differences of the $\tilde{c}_N(0)$ values does not have an effect of the dependences between the norm and the mean density $1 + \psi_0$ of the stable solution. But in figure 2.9 (b) and (c) it is to see that the mean densities of the low order models grows much faster with the chemical potential μ. Also the pressure differences of the solutions of the low order models groves faster with μ as the pressure differences of the higher order models.

The second solution of 4th order model have a much bigger periodic length as solutions of the models of the higher order models. The differences of this solution and the second solution of the DDFT model are so big, that the solution of the 4th order model can cause wrong assumptions about the solution of the DDFT model, if only the solution of the 4th order model is known.

The branch points of the second solutions of the other models are shifted a little bit. As for the solutions of the model (2.5) the mean density $1 + \psi_0$ and μ must be increased more to stimulate solutions with a periodic length of 1.095. This differences also decreases if the order N grows.

All in all, with the approximated PFC models (2.5) and (2.6) it is possible to make assumption about the periodic length of the solution of the DDFT model. With them it is possible to predict the type of bifurcations. It can be seen that the model (2.6) produces faster solutions, which fit better to the solution of the DDFT model, than the model (2.5).

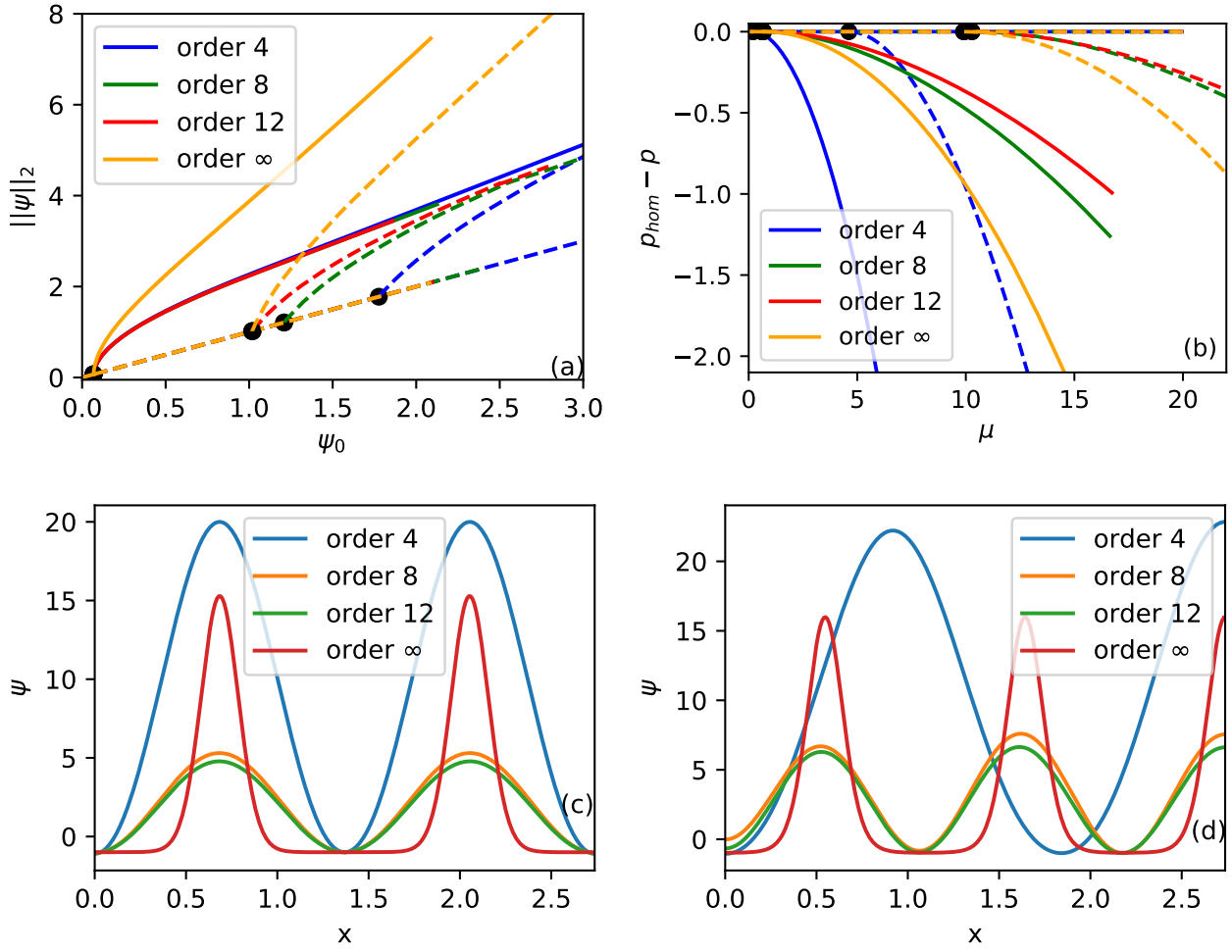

Figure 2.9: (a) Bifurcation diagram showing the norm of the solution of the PFC equation (2.6) as function of ψ_0 with $\eta = 2.5$. (b) Pressure difference between the uniform solution and the derived solution. (c) The solution of the PFC equation of branch 1. (d) The solution of the PFC equation of branch 2.
Here the stable solution of branch 1 of the PFC equation of low order is a cosine function with an periodic length of 1.369. The printed solution of 4th order has a chemical potential $\mu = 16.1$. The 8th order solution has a chemical potential of $\mu = 16.6$ and for the 12th order solution follows $\mu = 16.7$. The second solution of the 8th and 12th order model are cosine functions with an periodic length of 1.095. The 8th order solution has a chemical potential of $\mu = 26.3$ and the 12th order solution has $\mu = 25.8$. The 4th order solution has a periodic length of 1.82 and a chemical potential of $\mu = 20.5$

3 The Hard-Rod-PFC-Model

A model for hard particles of a diameter d and a further attractive interaction is studied in the 1D case in Refs. [14, 15]. An attractive potential is chosen with the energy

$$\mathcal{F}_{\mathsf{at}} = -\int_{-\infty}^{\infty} \mathrm{d}x \int_{-\infty}^{\infty} \mathrm{d}x' \frac{\alpha}{2} \exp(-\lambda|x - x'|)\rho(x)\rho(x') \tag{3.1}$$

Here α is the interaction strength and λ is the inverse range of this interaction.

The hard-rod energy is:

$$\mathcal{F}_{\mathsf{hr}} = -\frac{1}{2}\int_{-\infty}^{\infty} \mathrm{d}x\, k_B T \ln(1 - \eta[\rho](x))\left[\rho\left(x + \frac{d}{2}\right) + \rho\left(x - \frac{d}{2}\right)\right] \tag{3.2}$$

with

$$\eta[\rho](x) = \int_{x-\frac{d}{2}}^{x+\frac{d}{2}} \mathrm{d}x' \rho(x') \tag{3.3}$$

The total excess energy functional $\mathcal{F}_{\mathsf{exc}}$ is the sum of $\mathcal{F}_{\mathsf{at}}$ and $\mathcal{F}_{\mathsf{hr}}$.

3.1 The PFC-Model

To develop a PFC-model, the direct correlation functions $c^{(n)}(\vec{x})$ (1.14) are required. They are computed from the excess energy. Here, only the correlation function of second order $c^{(2)}(x, x') = c(x, x')$ is taken. It is split into an attractive part c_{at} and an hard-rod part c_{hc}. To obtain the attractive part, $\mathcal{F}_{\mathsf{at}}$ is functional-differentiated two times:

$$c_{\mathsf{at}} = \alpha\beta \exp(-\lambda|x_1 - x_2|) \tag{3.4}$$

To calculate c_{hc}, the second functional derivative of $\mathcal{F}_{\mathsf{hr}}$ has to be computed. The first variation is:

$$\frac{\delta \mathcal{F}_{\mathsf{hr}}[\rho(x)]}{\delta \rho(x_1)} = -\frac{k_B T}{2}\left[\ln\left(1-\int_{x_1}^{x_1+d}\mathrm{d}x'\rho(x')\right)+\ln\left(1-\int_{x_1-d}^{x_1}\mathrm{d}x'\rho(x')\right) - \int_{x_1-\frac{d}{2}}^{x_1+\frac{d}{2}}\mathrm{d}x\frac{\rho\left(x+\frac{d}{2}\right)+\rho\left(x-\frac{d}{2}\right)}{1-\int_{x-\frac{d}{2}}^{x+\frac{d}{2}}\mathrm{d}x'\rho(x')}\right] \tag{3.5}$$

Using

$$\frac{\delta}{\delta\rho(x_2)}\ln\left(1-\int_a^b \mathrm{d}x'\rho(x')\right) = -\frac{\Theta(x_2-a)\Theta(b-x_2)}{1-\int_a^b \mathrm{d}x'\rho(x')}$$

$$\frac{\delta}{\delta\rho(x_2)}\int_a^b \mathrm{d}x\frac{\rho\left(x+c\right)}{1-\int_{x-d}^{x+d}\mathrm{d}x'\rho(x')} = \frac{\Theta(x_2+c-a)\Theta(b-x_2-c)}{1-\int_{x_2+c-d}^{x_2+c+d}\mathrm{d}x'\rho(x')} + \int_a^b \mathrm{d}x\frac{\rho\left(x+c\right)\Theta(x_2-x+d)\Theta(x-x_2+d)}{\left(1-\int_{x-d}^{x+d}\mathrm{d}x'\rho(x')\right)^2}$$

the second functional derivation of $\mathcal{F}_{\mathsf{hr}}[\rho(x)]$ is:

$$\begin{aligned}\frac{\delta^2 \mathcal{F}_{\mathsf{hr}}[\rho(x)]}{\delta\rho(x_1)\delta\rho(x_2)} =& \frac{k_B T}{2}\left[\frac{\Theta(x_2-x_1)\Theta(x_1+d-x_2)}{1-\int_{x_1}^{x_1+d}\mathrm{d}x'\rho(x')}+\frac{\Theta(x_2-x_1+d)\Theta(x_1-x_2)}{1-\int_{x_1-d}^{x_1}\mathrm{d}x'\rho(x')}\right.\\ &+\frac{\Theta\left(x_2-x_1+d\right)\Theta\left(x_1-x_2\right)}{1-\int_{x_2}^{x_2+d}\mathrm{d}x'\rho(x')}+\frac{\Theta\left(x_2-x_1\right)\Theta\left(x_1-x_2+d\right)}{1-\int_{x_2-d}^{x_2}\mathrm{d}x'\rho(x')}\\ &\left.+\int_{x_1-\frac{d}{2}}^{x_1+\frac{d}{2}}\mathrm{d}x\frac{\rho\left(x+\frac{d}{2}\right)+\rho\left(x-\frac{d}{2}\right)}{\left(1-\int_{x-\frac{d}{2}}^{x+\frac{d}{2}}\mathrm{d}x'\rho(x')\right)^2}\Theta\left(x_2-x+\frac{d}{2}\right)\Theta\left(x-x_2+\frac{d}{2}\right)\right]\end{aligned} \tag{3.6}$$

$\Theta(x)$ is the heavy-side-function. It has to be considered, that the 1. and 4. term vanish here if $x_1 - x_2 \geq d$ or $x_1 - x_2 \leq 0$. The 2. and 3. vanish if $x_1 - x_2 \leq -d$ or $x_1 - x_2 \geq 0$. To compute the integrals it will be considered that the density is homogeneous ($\rho(x) = \rho_{\mathsf{ref}}(1+\psi_0) = \rho_0$). Then the correlation-function c_{hr} is:

$$c_{\mathsf{hr}} = -\frac{1-|\Delta x|\rho_0}{(1-d\rho_0)^2} \tag{3.7}$$

with $|\Delta x| = |x_1 - x_2| \leq d$.

To calculate the moments $\tilde{A}_{2\mu,r}$, we compute integrals of the form (1.24) and obtain

$$\tilde{A}_{2\mu,r} = \alpha\beta\frac{(2\mu)!}{\lambda^{2\mu+1}} - \frac{d^{2\mu+1}}{(1-d\rho_0)^2}\left(\frac{1}{2\mu+1} - \frac{d\rho_0}{2\mu+2}\right) \tag{3.8}$$

With these moments the PFC-equation of order $2M$ of the hard-rod model is

$$\partial_t\psi = D_T k_B T\partial_x^2\psi - D_T\partial_x(1+\psi)\partial_x\left(2\rho_{\text{ref}}\sum_{\mu=0}^{M}\left[\frac{\alpha}{\lambda^{2\mu+1}} - \frac{k_BT}{(2\mu)!}\frac{d^{2\mu+1}}{(1-d\rho_0)^2}\left(\frac{1}{2\mu+1} - \frac{d\rho_0}{2\mu+2}\right)\right]\partial_x^{2\mu}\psi\right) \tag{3.9}$$

Now $d\rho_0$ can be replaced by $\tilde{\rho}_0$ (i.e. $d\rho_{\text{ref}} = \tilde{\rho}_{\text{ref}}$), λd by ξ and $\frac{\alpha}{d\lambda k_BT}$ by $\tilde{\alpha}$. After scaling x with $\frac{1}{d}$ and t with $D_T\frac{k_BT}{d^2}$ the PFC-equation is

$$\partial_t\psi = \partial_x^2\psi - 2\tilde{\rho}_{\text{ref}}\,\partial_x(1+\psi)\partial_x\left(\sum_{\mu=0}^{M}\left[\frac{\tilde{\alpha}}{\xi^{2\mu}} - \frac{1}{(2\mu)!}\frac{1}{(1-\tilde{\rho}_0)^2}\left(\frac{1}{2\mu+1} - \frac{\tilde{\rho}_0}{2\mu+2}\right)\right]\partial_x^{2\mu}\psi\right) \tag{3.10}$$

3.2 Linear stability analysis of the homogeneous state

One fixed point of equation (3.10) is the homogeneous state of arbitraryψ_0. To discuss its stability, the ansatz $\psi(x,t) = \psi_0 + \varepsilon\exp(\gamma t + ikr)$ with $\varepsilon \ll 1$ is introduced into (3.10). Only terms of $\mathcal{O}(\varepsilon)$ are considered. The resulting dispersion relation $\gamma(k)$ is

$$\gamma_{2M}(k) = -k^2 - 2\tilde{\rho}_0k^2\sum_{\mu=0}^{M}\left[\frac{1}{(2\mu)!}\frac{1}{(1-\tilde{\rho}_0)^2}\left(\frac{1}{2\mu+1} - \frac{\tilde{\rho}_0}{2\mu+2}\right) - \frac{\tilde{\alpha}}{\xi^{2\mu}}\right](-k^2)^\mu \tag{3.11}$$

If $M\to\infty$, the sums can be expressed via trigonometric functions as

$$\sum_{m=0}^{\infty}\frac{(-1)^m}{(2m+1)!}k^{2m} = \frac{\sin(k)}{k} \tag{3.12}$$

$$\sum_{m=0}^{\infty}\frac{(-1)^m}{(2m)!}k^{2m}\frac{\tilde{\rho}_0}{2m+2} = \frac{\tilde{\rho}_0\sin(k)}{k} - \frac{\tilde{\rho}_0(1-\cos(k))}{k^2} \tag{3.13}$$

With these simplifications the dispersion relation is

$$\gamma(k) = -k^2 - \frac{2\tilde{\rho}_0k\sin(k)}{1-\tilde{\rho}_0} - \frac{4\tilde{\rho}_0^2\sin^2\left(\frac{k}{2}\right)}{(1-\tilde{\rho}_0)^2} + \frac{2\tilde{\rho}_0\tilde{\alpha}k^2}{1+\left(\frac{k}{\xi}\right)^2} \tag{3.14}$$

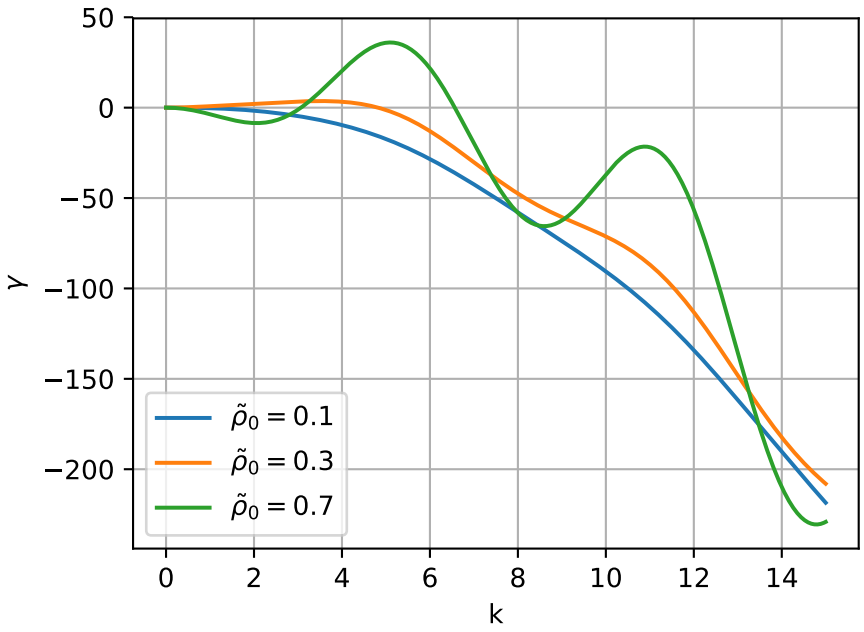

Figure 3.1: Dispersion-relation of the DDFT model (model of order ∞) with $\tilde{a} =$ and $\xi = 3$. For $\tilde{\rho}_0 = 0.1$ the homogeneous state is stable, for $\tilde{\rho}_0 = 0.3$ it is spinodal unstable and for $\tilde{\rho}_0 = 0.7$ it is freezing unstable

This is also the dispersion-relation from the DDFT [14, 15]. In figure 3.1 some dispersion relations of the DDFT model are shown. As it can be seen in this figure, the homogeneous state of the DDFT model can be stable (all $\gamma(k)$ values are negative). The homogeneous state can be spinodal instable ($\gamma(k)$ is positive around $k = 0$) or freezing unstable ($\gamma(k)$ is positive around $k = k_{\text{max}} \neq 0$).

3.2.1 Changes of the attractive term

One problem of the equation (3.11) is, that the attractive term does not converge for $\frac{k}{\xi} > 1$ (see fig. 3.2). To eliminate this problem, we chose a Gaussian attractive potential

$$\mathcal{F}_{\text{at}} = -\int_{-\infty}^{\infty} \mathrm{d}x \int_{-\infty}^{\infty} \mathrm{d}x' \frac{\alpha}{2} \cdot \exp(-(\lambda(x - x'))^2)\rho(x)\rho(x') \tag{3.15}$$

Then, the attractive part of the correlation function is

$$c_{\text{at}} = \alpha \cdot \exp(-(\lambda \Delta x)^2) \tag{3.16}$$

and the moments are

$$\tilde{A}_{2\mu,r} = \alpha\beta \frac{\sqrt{\pi}\mu!}{(\frac{\mu}{2})! 2^{\mu+1} \lambda^{2\mu+1}} - \frac{d^{\mu+1}}{(1 - d\rho_0)^2} \left(\frac{1}{\mu + 1} - \frac{d\rho_0}{\mu + 2} \right). \tag{3.17}$$

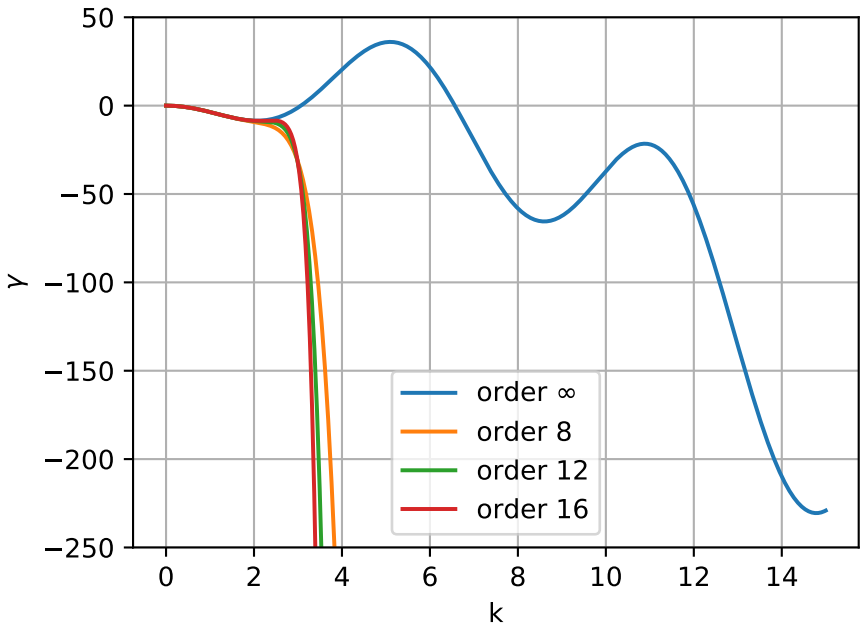

Figure 3.2: Dispersion-relation of the PFC model of different order with $\tilde{a} =$, $\tilde{\rho}_0 = 0.7$ and $\xi = 3$. For $k > 3$ the difference between $\gamma_\infty(k)$ and $\gamma_N(k)$ increase with the order N

The resulting PFC equation is

$$\partial_t \psi = k_B T \partial_x^2 \psi - \rho_{\text{ref}}\, \partial_x (1+\psi) \partial_x \left(\sum_{\mu=0}^{M} \left[\frac{\alpha\sqrt{\pi}}{\mu!(2\lambda)^{2\mu}\lambda} - \frac{k_B T}{(2\mu)!} \frac{2d^{2\mu+1}}{(1-d\rho_0)^2} \left(\frac{1}{2\mu+1} - \frac{d\rho_0}{2\mu+2} \right) \right] \partial_x^{2\mu} \psi \right) \tag{3.18}$$

In compare to the scaling of the PFC equation (3.10), the variables should be changed, such that $\tilde{\alpha} = \frac{\alpha\sqrt{\pi}}{2d\lambda k_B T}$:

$$\partial_t \psi = \partial_x^2 \psi - 2\tilde{\rho}_{\text{ref}}\, \partial_x (1+\psi) \partial_x \left(\sum_{\mu=0}^{M} \left[\frac{\tilde{\alpha}}{\mu!(2\xi)^{2\mu}} - \frac{1}{(2\mu)!} \frac{1}{(1-\tilde{\rho}_0)^2} \left(\frac{1}{2\mu+1} - \frac{\tilde{\rho}_0}{2\mu+2} \right) \right] \partial_x^{2\mu} \psi \right) \tag{3.19}$$

The dispersion relation becomes

$$\gamma_{2M}(k) = -k^2 - 2k^2 \tilde{\rho}_0 \sum_{\mu=0}^{M} \left[\frac{1}{(2\mu)!} \frac{1}{(1-\tilde{\rho}_0)^2} \left(\frac{1}{2\mu+1} - \frac{\tilde{\rho}_0}{2\mu+2} \right) - \frac{\tilde{\alpha}}{\mu!(2\xi)^{2\mu}} \right] (-k^2)^\mu \tag{3.20}$$

and can for $M \to \infty$, be written as

$$\gamma(k) = -k^2 - \frac{2\tilde{\rho}_0 k \sin(k)}{1-\tilde{\rho}_0} - \frac{4\tilde{\rho}_0^2 \sin^2\left(\frac{k}{2}\right)}{(1-\tilde{\rho}_0)^2} + 2\tilde{\alpha}\tilde{\rho}_0 k^2 \exp\left(-\left(\frac{k}{2\xi}\right)^2\right) \tag{3.21}$$

3.3 Stability diagram of the hard rod model

The homogeneous state of the hard rod model becomes linearly unstable if the dispersion relation (3.20) is positive for some range of wavenumber k. This can have 2 reasons.

First, the prefactor of the 2nd order term become positive:

$$0 < -1 - 2\tilde{\rho}_0 \left[\frac{1}{(1-\tilde{\rho}_0)^2}\left(1 - \frac{\tilde{\rho}_0}{2}\right) - \tilde{\alpha}\right] \tag{3.22}$$

This equation follows from eq. (3.20) for $M = 0$. In this case, a band of wavenumbers around $k = 0$ becomes unstable (see dispersion relation for $\tilde{T} = 0.25$ in Fig. 3.5). This is the spinodal instability corresponding to the liquid-gas transition. The phase border can be defined analytically by reformulating equation (3.22)

$$\frac{1}{\tilde{a}} = \tilde{T} < 2\tilde{\rho}_0(1-\tilde{\rho}_0)^2. \tag{3.23}$$

Here, $\tilde{T}$ is the scaled temperature. The maximum of this curve is at $\tilde{\rho}_0 = \frac{1}{3}$ with $\tilde{T} = \frac{8}{27}$ and corresponds to the critical point. Because the spinodal instability only depends on the 2nd order term of the dispersion relation and all discussed PFC-equations include an identical 2nd order term, the instability border Eq. (3.23) is independent of the order N of the model. The scaling of $\tilde{a}$ is chosen, such that this model and the model of (3.10) have the same 2nd order prefactor [14]. Note that (3.23) in Ref. [14] has a typo.

Second, the freezing instability sets in a k-range centered about a finite k_{max} bound away from zero, with $\gamma_N(k_{\mathsf{max}}) \geq 0$ (see dispersion relation for $\tilde{T} = 0.333$ and $\tilde{T} = 0.4$ in Fig. 3.5). This corresponds to the onset of crystallisation as discussed in section 2.2 for the GEM4 model. The border of this instability can not be computed analytically.

One problem for the computation is , that the position of the maximum k_{max} of the dispersion relation depends on the values $\tilde{T}$ and $\tilde{\rho}_0$. As it can be seen in figure 3.3, k_{max} depends especially on the mean density $\tilde{\rho}_0$.

To calculate these borders, arclength continuation described in section 1.5 can be used.

We start with a homogeneous state, which is not spinodally unstable. The first maximum at $k_{\mathsf{max}} \neq 0$ of the dispersion relation of this state should have a value zero. So it follows that a root of

$$\vec{f}(k_{\mathsf{max}}, \tilde{a}, \tilde{\rho}_0) = \begin{pmatrix} \gamma_N(k_{\mathsf{max}}, \tilde{a}, \tilde{\rho}_0) \\ \partial_k \gamma_N(k_{\mathsf{max}}, \tilde{a}, \tilde{\rho}_0) \end{pmatrix} \tag{3.24}$$

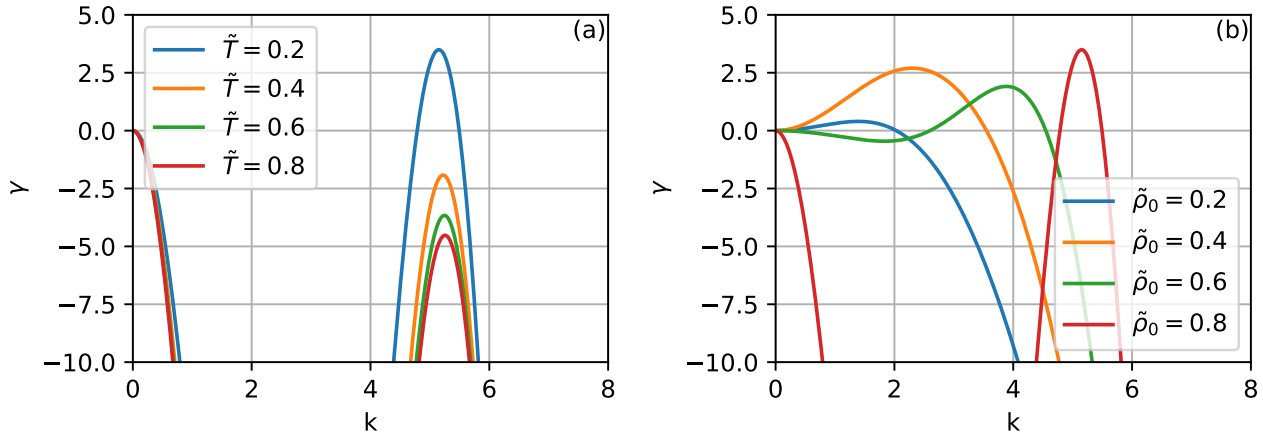

Figure 3.3: Dispersion relation of the homogeneous state for the hard rod model with $\xi = 1.5$.
(a): $\tilde{\rho}_0 = 0.8$ different $\tilde{T}$.
(b): $\tilde{T}_0 = 0.2$ different $\tilde{\rho}_0$
$\tilde{T}$ change the hight of the maxima and $\tilde{\rho}_0$ the hight and the k position

has to be found. The Jacobian matrix of $\vec{f}(k_{\text{max}}, \tilde{a}, \tilde{\rho}_0)$ is

$$J_f(k_{\text{max}}, \tilde{a}, \tilde{\rho}_0) = \begin{pmatrix} \partial_k \gamma_N(k_{\text{max}}, \tilde{a}, \tilde{\rho}_0) & \partial_{\tilde{a}} \gamma_N(k_{\text{max}}, \tilde{a}, \tilde{\rho}_0) \\ \partial_k^2 \gamma_N(k_{\text{max}}, \tilde{a}, \tilde{\rho}_0) & \partial_k \partial_{\tilde{a}} \gamma_N(k_{\text{max}}, \tilde{a}, \tilde{\rho}_0) \end{pmatrix} \tag{3.25}$$

Here, $\tilde{\rho}_0$ is the continuation parameter. Because for $N \to \infty$ the amplitude of $\tilde{c}_{\text{hr}}(k)$ and $\tilde{c}_{\text{at}}(k)$ decrease with respect to k, the second maximum can be neglected in the discussion of a stability diagram. The same follows for the PFC model of order $N \neq \infty$.

In Ref. [14] it can be seen, that the uniform solution of the model in eq. (3.10) can become spinodal and freezing instable at the same time. As mentioned before, the freezing instability border can not be computed analytically. But the existence of this coexistence of instabilities can be excluded for a specific $\tilde{\rho}_0$ range.

Therefor the dispersion relation (3.20) will be divided by k^2.

$$f(k) = -1 - 2\tilde{\rho}_0 \sum_{\mu=0}^{M} \left[\frac{1}{(2\mu)!} \frac{1}{(1-\tilde{\rho}_0)^2} \left(\frac{1}{2\mu+1} - \frac{\tilde{\rho}_0}{2\mu+2} \right) - \frac{\tilde{\alpha}}{\mu!(2\xi)^{2\mu}} \right] (-k^2)^\mu \tag{3.26}$$

Except for $k = 0$, this equation has the same zero points and $f(k) > 0$ if the dispersion relation $\gamma_{2M}(k) > 0$. At the spinodal border $\tilde{T} = 2\tilde{\rho}_0(1-\tilde{\rho}_0)^2$ the function at $k = 0$ has the value $f(0) = 0$. Because the function $f(k)$ is inversion invariant, for the coexistence follows, that the prefactor of whose 2nd order term has to be negative at region next to the spinodal border. In this case, $k = 0$ is a local maximum of $f(k)$ and if the temperature $\tilde{T}$ is a little bit smaller as the border $2\tilde{\rho}_0(1-\tilde{\rho}_0)^2$, a minimum between $k = 0$ and the first main maximum k_{max} of the dispersion relation, which is smaller than zero, can occur. Otherwise if $f(k)$ has a minimum at $k = 0$ the dispersion relation increase monotonic between $k = 0$ and k_{max}. This can be seen in figure 3.4.

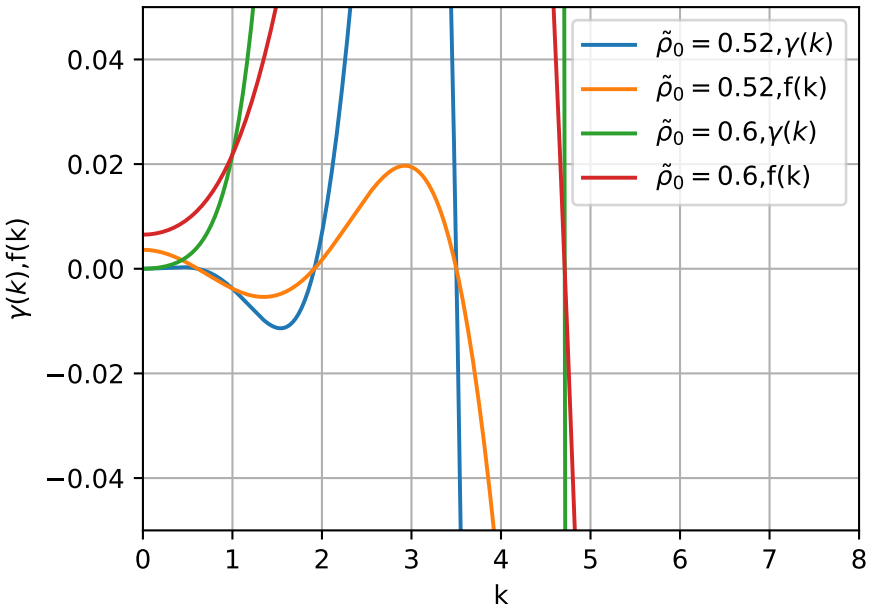

Figure 3.4: Dispersion relation and $f(k)$ next to the spinodal border. $\xi = 1.52$. The difference between $\tilde{T}$ and $2\tilde{\rho}_0(1-\tilde{\rho}_0)^2$ is -0.0002. For $\tilde{\rho}_0 = 0.52$ a coexistence of the spinodal and the freezing instability is possible. For $\tilde{\rho}_0 = 0.6$ a coexistence is impossible.

So for the coexistence follows

$$0 < \frac{1}{2}\frac{1}{(1-\tilde{\rho}_0)^2}\left(\frac{1}{3} - \frac{\tilde{\rho}_0}{4}\right) - \frac{1}{4\xi^2}\frac{1}{2\tilde{\rho}_0(1-\tilde{\rho}_0)^2} \tag{3.27}$$

In the definition space $0 < \tilde{\rho}_0 < 1$ this condition can be reformed in

$$0 < -\tilde{\rho}_0^2 + \frac{4}{3}\tilde{\rho}_0 - \frac{1}{\xi^2}. \tag{3.28}$$

The quadratic equation has the solutions

$$\tilde{\rho}_0 = \frac{2}{3} \pm \sqrt{\frac{4}{9} - \frac{1}{\xi^2}} \tag{3.29}$$

It follows, that if the width of the attractive part $\xi < \frac{3}{2}$, the equation has no real solution and the condition (3.28) is fulfilled for each $\tilde{\rho}_0$ value. It can not be excluded, that a coexistence exist. If $\xi > \frac{3}{2}$ the condition (3.28) will be broken between the two solutions. So between the two points, a coexistence of the spinodal and freezing instability can be excluded.

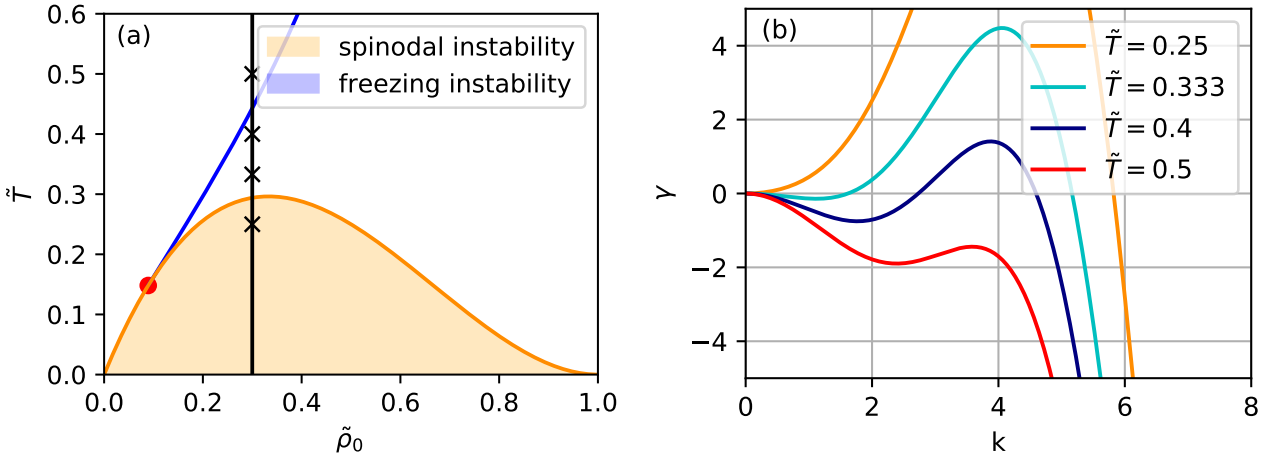

Figure 3.5: (a):Stability diagram of the hard rod model of order ∞ with $\xi = 3$. The red point is the emerging point of the freezing instability border from the spinodal instability border (triple point).
(b): Dispersion relations of the homogeneous state for the hard rod model with $\xi = 3$ and $\tilde{\rho}_0 = 0.3$ at the black crosses in (a). For $\tilde{T} = 0.5$ the system is stable, for $\tilde{T} = 0.333$ and $\tilde{T} = 0.4$ freezing unstable and for $\tilde{T} = 0.25$ spinodal unstable.
$\tilde{T} = \frac{1}{\tilde{a}}$.

3.3.1 Stability diagram of the model of order ∞

First, we start with the stability diagram of the DFT model with $\xi = 3$. Our starting point is at $(\tilde{\rho}_0, \frac{1}{\tilde{a}}, k_{\text{max}}) = (0.5, 0.832, 4.454)$ and we decrease $\tilde{\rho}_0$. At the triple point (Fig 3.5), the sign of $\Delta\tilde{\rho}_0$ changes and the algorithm continues in the $+\tilde{\rho}_0$ direction.

The mentioned triple point is one of the solutions of Eq. (3.28) ($\tilde{\rho}_0 = \frac{2}{3} - \sqrt{\frac{1}{3}}$). This solution is the single solution inside the definition space ($0 < \tilde{\rho}_0 < 1$). At the triple point the the freezing instability border bifurcate from the spinodal instability border.

As it can be seen in figure 3.6, the maximum position k_{max} converge to zero if $\tilde{\rho}_0$ goes to the triple point $\tilde{\rho}_0 = \frac{3}{2} - \sqrt{\frac{1}{3}}$. For $\tilde{\rho}_0 < \frac{3}{2} - \sqrt{\frac{1}{3}}$ the uniform solution can not become freezing unstable. So it follows that for $\xi = 3$, that a coexistence of the freezing and the spinodal instability does not exist.

To get a stability diagram with an overlapping region of the two instabilities (compare to the model with the exponential function Ref. [14]), ξ must be decreased. In figure 3.7 the stability diagram of the hard rod model with $\xi = 1.5$ is shown. For this value the two instabilities overlap, but compared to Ref. [14] this region is very small.

In figure 3.8 dispersion relations of homogeneous states with $\xi = 1.5$ and $\tilde{\rho}_0 = 0.54$ are shown. As it can be seen in the figure, there exist homogeneous states, which are freezing and spinodal unstable.

In figure 3.6 the k-position of the extrema depending on $\tilde{\rho}_0$ is shown. The algorithm starts at the border between the freezing instability and the stable region. Here k_{ext} is the first maximum of the dispersion relation with $\gamma(k_{\text{ext}}) = 0$. During the algorithm $\tilde{\rho}_0$ and k_{ext} decrease at the same time. If $\tilde{\rho}_0$ will be decreased and the freezing instability border cross the spinodal border, an additional maximum between

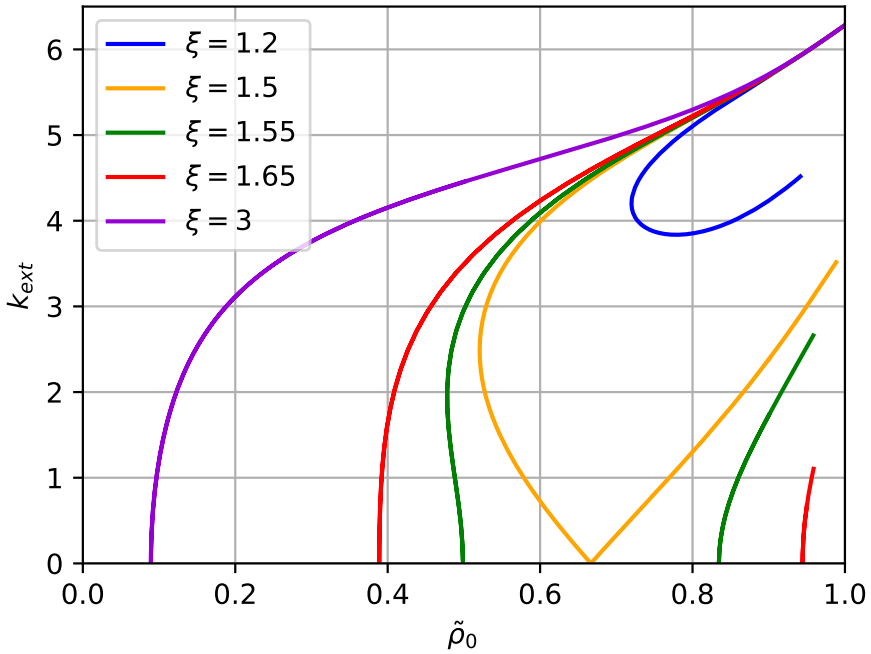

Figure 3.6: Position of maxima and minima at the freezing instability border (the blue line in the stability diagrams fig. 3.5 and 3.7). If one model has for a given $\tilde{\rho}_0$ value two different k_{ext} values, than the model has a coexistence region of the spinodal and the freezing instability region at $\tilde{\rho}_0$. In this case the high k_{ext} value is a maximum and the low value is the first minimum. If a model has only one solution for k_{ext}, a coexistence does not exist and k_{ext} is the first maximum. If a model has for a given $\tilde{\rho}_0$ no solution for k_{ext}, the system can not become freezing unstable.

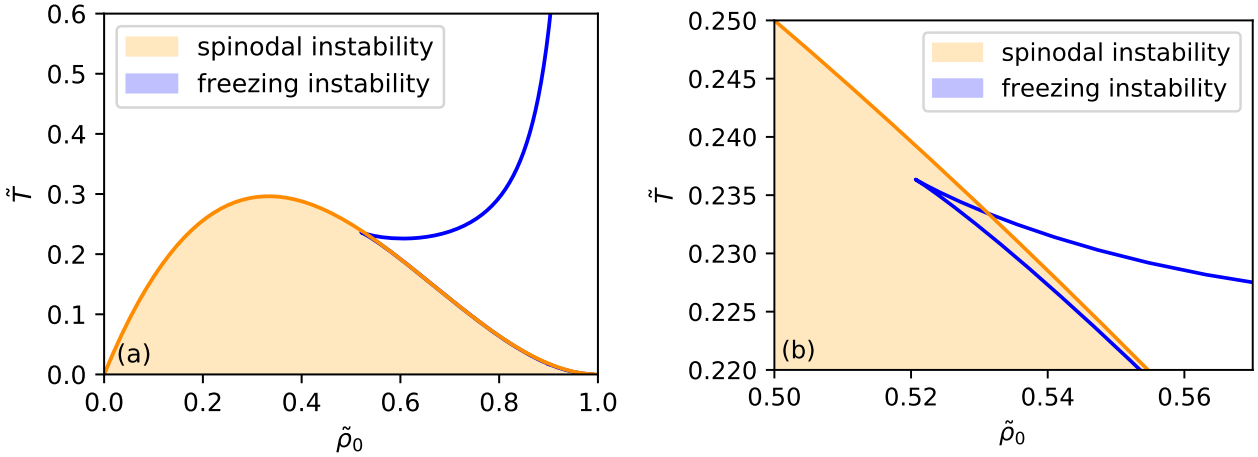

Figure 3.7: Stability diagram of the hard rod model of order ∞ with $\xi = 1.5$. The spinodal and the freezing instability region overlap.
(a):The full stability diagram
(b):The stability diagram, magnified at the overlapping region of the spinodal and the freezing instability

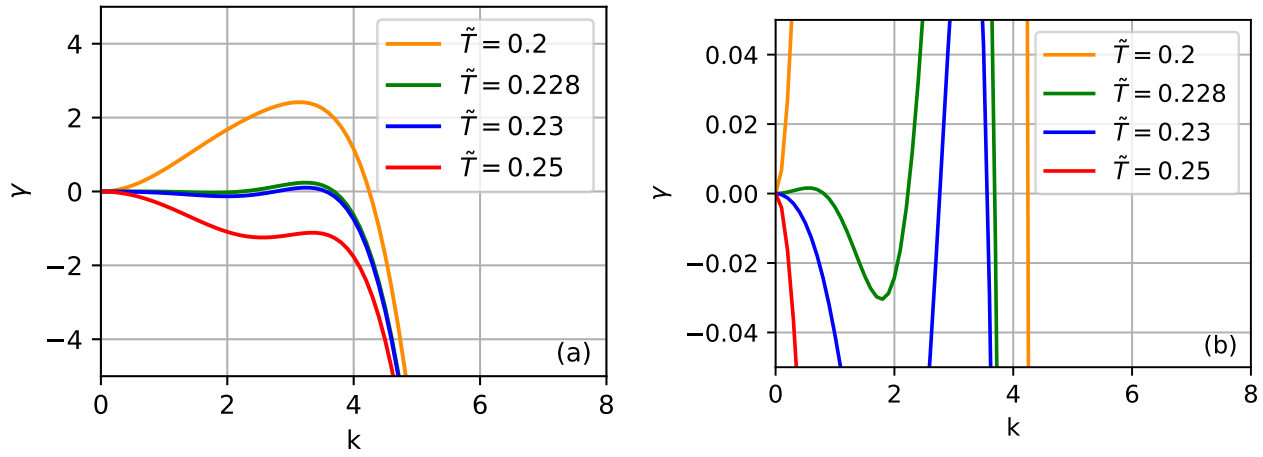

Figure 3.8: Dispersion relation of the homogeneous state for the hard rod model with $\xi = 1.5$ and $\tilde{\rho}_0 = 0.54$. For $\tilde{T} = 0.25$ the system is stable, for $\tilde{T} = 0.23$ freezing unstable and for $\tilde{T} = 0.2$ spinodal unstable. For $\tilde{T} = 0.228$ the system is freezing and spinodal unstable.
(a) The full dispersion relation.
(b) The dispersion relation, magnified at $\gamma = 0$

$k = 0$ and the observed maximum k_{ext} arise (see figure 3.8 (b) with $\tilde{T} = 0.228$). So k_{ext} becomes the second maximum.

At $\tilde{\rho}_0 \approx 0.52$ the instability border has a turning point. This point can be compared with a fold point in a bifurcation diagram. If $\tilde{\rho}_0$ will be decreased and converge to the fold point the k distance between the second maximum k_{ext} and the first minimum decreases. At the fold point the maximum and the minimum emerge. In the algorithm k_{ext} change the role and become the first minimum at the fold point.

After the fold point k_{ext} will be decreased even more. At $\tilde{\rho}_0 = \frac{2}{3}$, the single solution of Eq. (3.28) with $\xi = \frac{3}{2}$, k_{ext} cross the x-axes. At the same point the freezing instability border bifurcate two times from the spinodal instability border. As it can be seen also figure 3.12, the difference between spinodal and the freezing instability border is zero at $\tilde{\rho}_0 = \frac{2}{3}$. After this double bifurcation point k_{ext} grows again.

For $\xi = 1.2$ the system has for a given $\tilde{\rho}_0$ always two or none solution for the k_{ext}-position for the extrema. It follows for this ξ, that if the system can become freezing instable for a given $\tilde{\rho}_0$, the system can also become spinodal instable at the same time.

Next, we choose widths of the attractive term ξ, which is located between $\frac{3}{2}$ and $\sqrt{3}$. So it will be analyzed what happens if the equation (3.28) has two solutions. In fig. 3.6 also, the extrema of the models with $\xi = 1.55$ and $\xi = 1.65$ are shown. Both models have coexistence regions, but as for the model with $\xi = 1.5$ these regions are very small. With the solutions for the $\xi = 1.5$ and $\xi = 3$ model, it can be made analogies to the discussed models.

For $\tilde{\rho}_0 > \frac{3}{2} + \sqrt{\frac{9}{4} - \frac{1}{\xi}^2}$, the $\xi = 1.55$ and $\xi = 1.65$ model have two derived solutions for k_{ext} in the definition space. The high k-value is the first maximum of the dispersion relation at the border between the stable and the freezing instable region. The low k-value is the first minimum of the dispersion relation at the border of the coexistence region. Theoretically this solution can be found for all $\tilde{\rho}_0$ values which are smaller than one. It follows that for $\frac{3}{2} < \xi < \sqrt{3}$ the model has a coexistence region at $\tilde{\rho}_0 > \frac{3}{2} + \sqrt{\frac{9}{4} - \frac{1}{\xi}^2}$.

For $\xi = 1.55$ the first solution has a course, which has the form of a fold point. So for a small region with $\tilde{\rho}_0 < \frac{3}{2} - \sqrt{\frac{9}{4} - \frac{1}{\xi}^2}$, the system has two solutions for k_{ext}. It follows that in this region, the system has also a coexistence region. For $\xi = 1.65$ the solution has not a fold point. So the solution has the shape of the solution for $\xi = 3$. It follows, that for $\xi = 1.65$ the system only has one overlapping region.

Now the question is, if it is possible to predict, if a overlapping region next to a bifurcation point exist or not. If this region exist, the analyzed k_{ext} (fig. 3.6) next to the point must be the first minimum, which is equal to zero. As mentioned before, the derived maximum position k_{ext} is always bigger then the minimum position. At a bifurcation point next to a coexistence region, the maximum position is bigger than zero. So at the point, the dispersion relation should have a minimum at $k = 0$. As defined the bifurcation points before, the second and fourth order term of the dispersion relation is equal to zero. So to get a minimum at $k = 0$, the prefactor of sixth order term (plug in the $\mu = 2$ term of the Fourier-transformed correlation of eq. (3.20)) must be positive.

$$0 > -2\tilde{\rho}_0 \left[\frac{1}{4!} \frac{1}{(1-\tilde{\rho}_0)^2} \left(\frac{1}{5} - \frac{\tilde{\rho}_0}{6} \right) - \frac{\tilde{\alpha}}{2(2\xi)^4} \right] \tag{3.30}$$

with $\frac{1}{\tilde{\alpha}} = \tilde{T} = 2\tilde{\rho}_(1-\tilde{\rho}_0)^2$ and eq. (3.28) follows

$$\begin{aligned} \frac{1}{\xi^2} &= \frac{4}{3}\tilde{\rho}_0 - \tilde{\rho}_0^2 \\ 0 &> \tilde{\rho}_0^2 - \frac{6}{5}\tilde{\rho}_0 + \frac{9}{4\xi^4} = \frac{9}{4}\left(\tilde{\rho}_0^4 - \frac{8}{3}\tilde{\rho}_0^3 + \frac{16}{9}\tilde{\rho}_0^2 \right) + \tilde{\rho}_0^2 - \frac{6}{5}\tilde{\rho}_0 \end{aligned}$$

If ξ is finite, $\tilde{\rho}_0 = 0$ can not solve the condition (3.29). So it follows

$$0 > \frac{9}{4}\tilde{\rho}_0^3 - 6\tilde{\rho}_0^2 + 5\tilde{\rho}_0 - \frac{6}{5} \tag{3.31}$$

This cubic equation has only the real solution $\tilde{\rho}_0 \approx 0.413$. This means, that if the $\tilde{\rho}_0$ position of a bifurcation point is bigger than 0.413, the bifurcating freezing instability border has a lower temperature $\tilde{T}$ than the spinodal instability border and the system has a coexistence region next to this bifurcation point. It follows, that the solution $\tilde{\rho}_0 = \frac{2}{3} + \sqrt{\frac{4}{9} - \frac{1}{\xi^2}}$ of the condition (3.28) always fulfills the condition (3.31). The second solution $\tilde{\rho}_0 = \frac{2}{3} - \sqrt{\frac{4}{9} - \frac{1}{\xi^2}}$ fulfills the condition (3.31), if $\xi < 1.622$.

To sum it up, if $\xi \leq \frac{3}{2}$, follows that if the system can become freezing instable for a given $\tilde{\rho}_0$, the system can become spinodal instable at the same time. If $\xi > \frac{3}{2}$ the coexistence region will be split in two separate areas. For $\frac{2}{3} - \sqrt{\frac{4}{9} - \frac{1}{\xi^2}} < \tilde{\rho}_0 < \frac{2}{3} + \sqrt{\frac{4}{9} - \frac{1}{\xi^2}}$ the spinodal and the freezing instabilities can not coexist at the same time. For $\xi > 1.622$ the coexistence region next to $\tilde{\rho}_0 = \frac{2}{3} - \sqrt{\frac{4}{9} - \frac{1}{\xi^2}}$ vanishes. If $\xi \geq \sqrt{3}$ the solution $\tilde{\rho}_0 = \frac{2}{3} + \sqrt{\frac{4}{9} - \frac{1}{\xi^2}}$ is outside the definition space and the spinodal and freezing instability can not coexist at the same time.

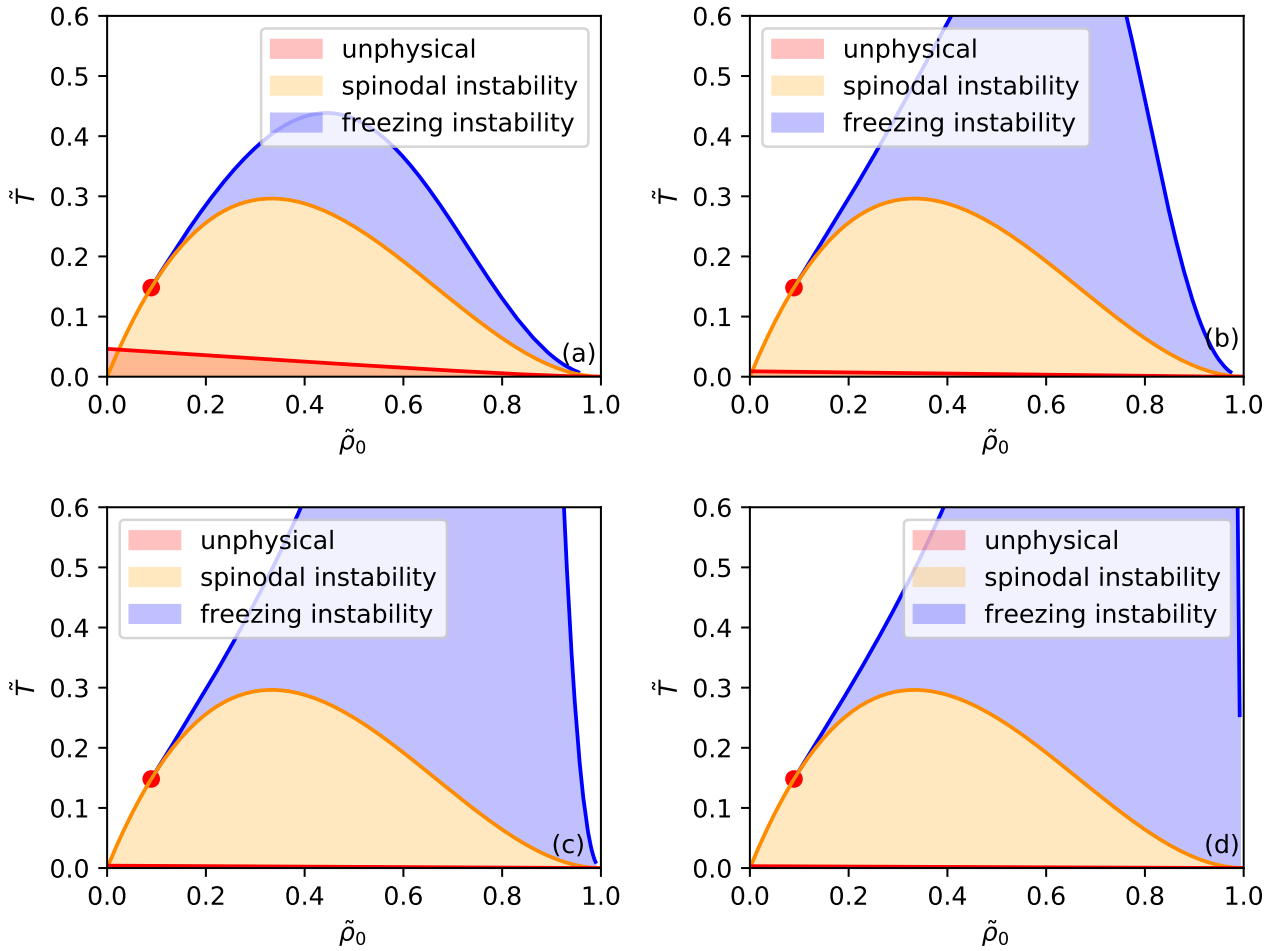

Figure 3.9: Stability diagram of the hard rod model with $\xi = 3$.
(a): 4th order,(b): 8th order,(c): 12th order,(d): 16th order
All triple points are at the same position. The region of the freezing instability becomes bigger with increasing order N

3.3.2 Stability diagram of the model of order N

Before the border of the freezing instable region is computed, it has to be considered, that the dispersion relation is always negative for $k \to \infty$. Otherwise the system is unphysical. A system is unphysical, if the highest order term is negative. If $N = 2M$ is the order of the system, the highest order term is zero if

$$\tilde{T} = \tilde{T}_{\text{er}} = \frac{(2M+2)!}{M!} \left(\frac{1-\tilde{\rho}_0}{(2\tilde{\rho}_0)^M} \right)^2 \frac{1}{2M+2-(2M+1)\tilde{\rho}_0}. \tag{3.32}$$

Because the highest order term of the dispersion relation is proportional to $(-k^2)^M$ the system is physically reasonable for an even M if $\tilde{T} > \tilde{T}_{\text{er}}$ and for an odd M if $\tilde{T} < \tilde{T}_{\text{er}}$.

First, the stability diagrams of the approximated models with $\xi = 3$ will be discussed. As mentioned before, it can be seen in figure 3.9, that all models have the same triple point ($\tilde{\rho}_0 = \frac{2}{3} - \sqrt{\frac{1}{3}}$). But with a growing

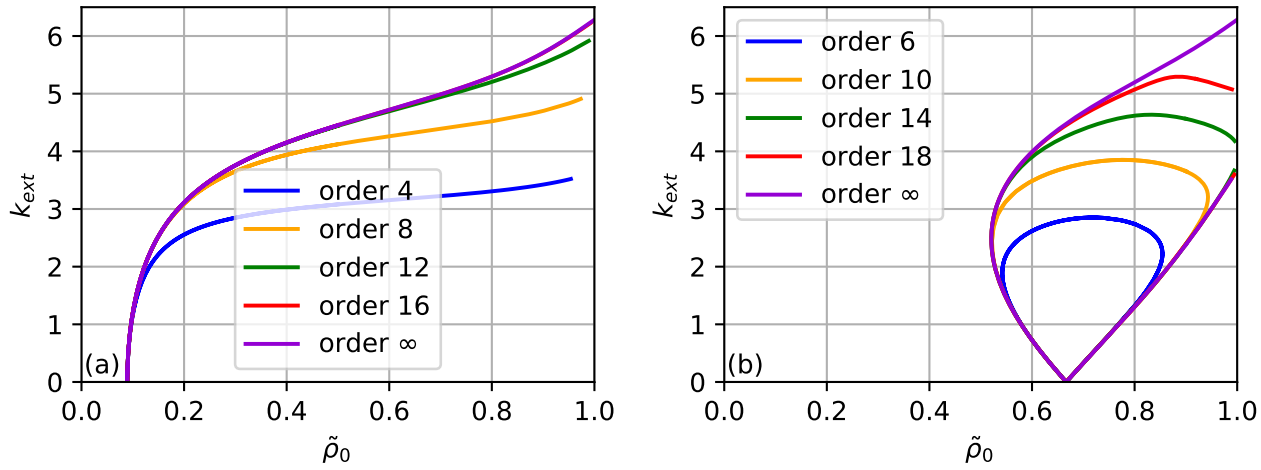

Figure 3.10: k position of the extrema depending on $\tilde{\rho}_0$ at the border of the freezing instability (blue line in figure 3.5, 3.7, 3.9,3.11).
(a) $\xi = 3$: If $\tilde{\rho}_0 \to \frac{2}{3} - \sqrt{\frac{1}{3}}$ (at the triple point) all $k_{\text{max}} \to 0$.
(b) $\xi = 1.5$: Start on the first maximum of the dispersion relation and decrease the temperature. At the turning points (for the order ∞ at $\tilde{\rho}_0 \approx 0.52$) k_{ext} becomes the minimum between $k = 0$ and the first maximum. For $\tilde{\rho}_0 \to \frac{2}{3}$ all minima goes to zero.

$\tilde{\rho}_0$ and decreasing order N the difference between the freezing instability borders grows.

In Fig. 3.10 it can be seen, that $k_{\text{max}} \to 0$ if we converge to the triple point. Because the position of this point only depends on the 4th order term of the dispersion relation, and can be computed by (3.29), this position does not depend on the order number N of the model. In the subsection 3.3.1, it is shown, that the bifurcation direction of the freezing instability border from the spinodal instability border depends on the 6th order term of the dispersion relation. All models have the same or a higher order number. So the direction also does not depend on the order number. Because the Fourier-expanded correlation function is expanded about $k = 0$ the differences decrease if $|k|$ decreases.

At higher densitys $\tilde{\rho}_0$ the differences between maxima position of the PFC models of small order N and the DDFT model become larger. In the PFC models the k_{max} position is for high densities $\tilde{\rho}_0$ smaller than in k_{max} position DDFT model. For higher densities the height of the maxima of also decrease, if $\tilde{T}$ is constant . As seen in figure 3.3, the temperature $\tilde{T}$ must fall to raise the height of these maxima again, and get a system which have a first maximum which is equal to zero. For models of higher orders, these differences become neglectable.

Here, only systems with order $N = 4M$ with $M \in \mathbb{N}$ are physical (with an negative highest order term) in the region near by the triple point. For very high M, the order $4M$ terms become positive close to the triple point and a system of order $N = 4\tilde{M}$ with $\tilde{M} \geq M$ becomes unphysical. So for these high order models only models of order $N = 4\tilde{M} + 2$ are physical.

Next, the diagrams with $\xi = 1.5$ are analyzed. In figure 3.11 we see, that for the low order models, the freezing instability region is very small and that this region grows very slowly with the order N.

Inside the spinodal instability region, the freezing instability border does not differ much form the spinodal instability border. To analyze the freezing instable border inside the spinodal instability region better, we

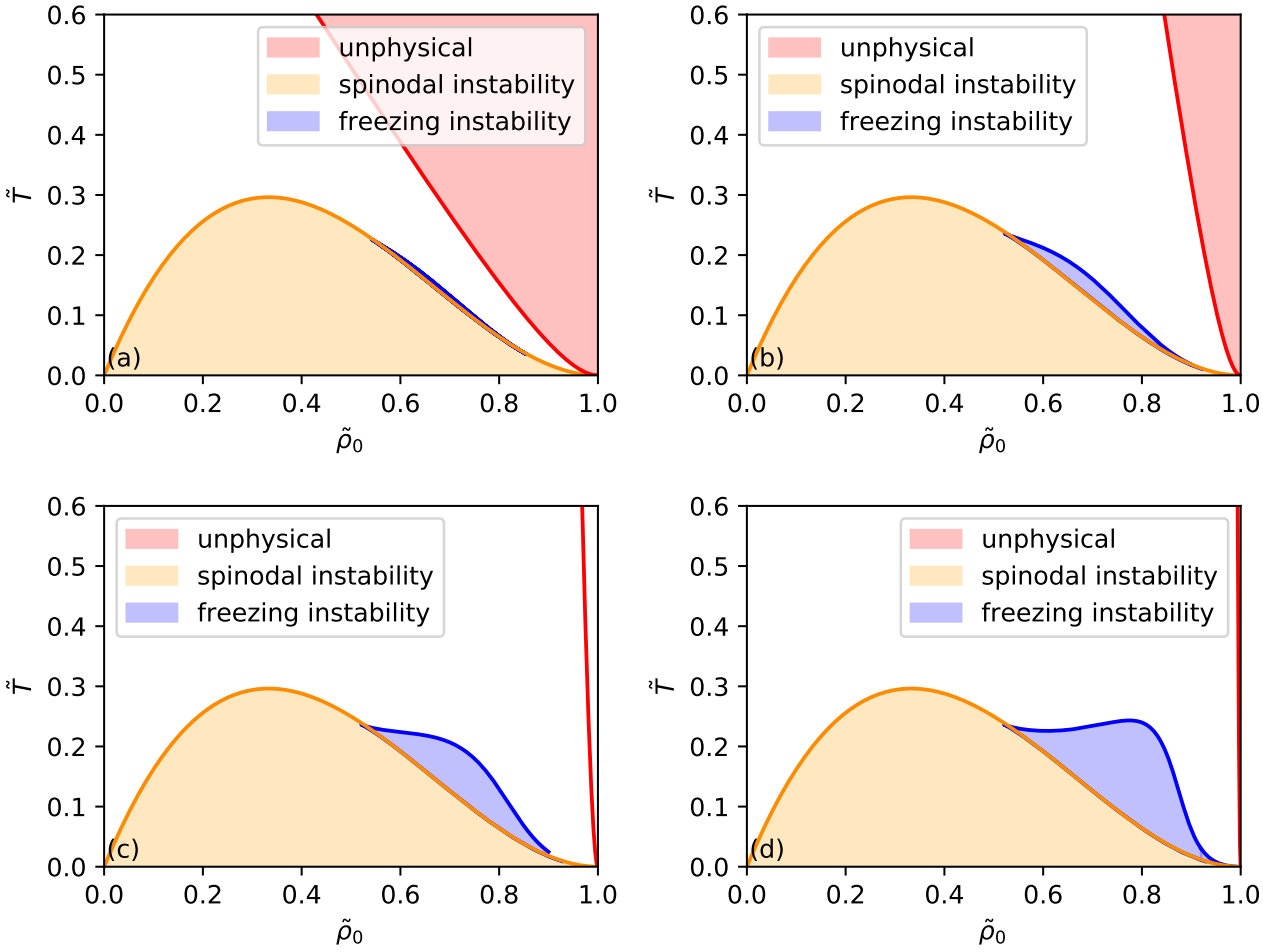

Figure 3.11: Stability diagram of the hard rod model with $\xi = 1.5$.
(a) 6th order,(b) 10th order,(c) 14th order,(d) 18th order

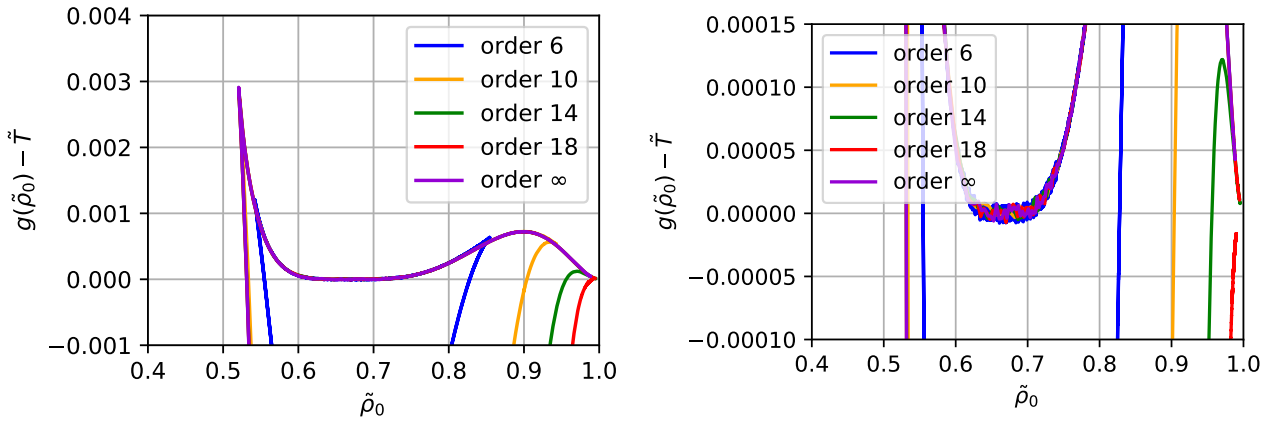

Figure 3.12: Comparision of the freezing instability border $\tilde{T}$ with the spinodal instability border $g(\tilde{\rho}_0) = 2\tilde{\rho}_0(1-\tilde{\rho}_0)^2$ for $\tilde{T}$ lays in the spinodal instable region. Only for the 6th order model the first turning point differ clearly from the turning point of the DDFT model (order ∞). In contrast to the DDFT model the approximated models have a second turning point. Between the turning points all borders of the approximated models does not differ much from the border of the DDFT model.

print the difference between spinodal and the freezing instability borders in figure 3.12. So it is also possible to differ between the freezing instability borders of different models. In the spinodal instability region the differences between the freezing instable borders of different order models are smaller as outside the spinodal instable region. In contrast to the DDFT model, the approximated models have a second turning point, and also the first turning point of the 6th order model differ clearly from the turning point of the order ∞ model. As defined in subsection 3.3.1, turning points have the shape of a fold point in a bifurcation diagram. But between these turning points the differences between the borders of the DDFT model and the approximated models are negligibly small.

In figure 3.10 we also show the position of the first extremum of the dispersion relation at the freezing instability border with $\xi = 1.5$. Between the turning points the algorithm computed two extrema of the system for the same density $\tilde{\rho}_0$. The higher k-values are the maximum and the lower values are the first minimum. If the system is outside the spinodal instability region, the higher k-values are the first maximum and inside this region the second maximum. As in subsection 3.3.1 all turning points are inside the spinodal instability region. At the turning points the maximum and the minimum have the same position and in the algorithm the role of the maximum and the minimum changes. Beyond of this region the homogeneous state can not become freezing instable.

The 6th and 10th order model have two turning points in the definition space of $\tilde{\rho}_0$ $(0 < \tilde{\rho}_0 < 1)$. So the uniform state can not become freezing instable if the density is to low (as in the DDFT model) or to high. The higher order models does not have a second turning point in the definition space.

In figure 3.10 it can be also seen, that the minimum position converge to zero if $\tilde{\rho}_0$ goes to $\frac{2}{3}$. This point does not depend on the order N. As it can be seen in figure 3.12, the differences between the spinodal and freezing instability border become very small around $\tilde{\rho}_0 = \frac{2}{3}$.

Bibliography

[1] Y. Singh. Density-functional theory of freezing and properties of the order phase. *Phys. Rep.*, 207:351–444, 1991.

[2] H. Emmerich, H. Löwen, R. Wittkowski, T. Gruhn, G. I. Tóth, G. Tegze, and L. Gránásy. Phase-field-crystal models for condensed matter dynamics on atomic length and diffusive time scales: an overview. *Adv. Phys.*, 61:665–743, 2012.

[3] R. Evans. The nature of the liquid-vapour interface and other topics in the statistical mechanics of non-uniform, classical fluids. *Adv. Phys.*, 28:143–200, 1979.

[4] T. V. Ramakrishnan and M. Yussouff. First-principles order-parameter theory of freezing. *Phys. Rev. B*, 19:2775–2794, 1979.

[5] A. J. Archer and R. Evans. Dynamical density functional theory and its application to spinodal decomposition. *J. Chem. Phys.*, 121:4246–4254, 2004.

[6] H. A. Dijkstra, F. W. Wubs, A. K. Cliffe, E. Doedel, I. F. Dragomirescu, B. Eckhardt, A. Y. Gelfgat, A. Hazel, V. Lucarini, A. G. Salinger, E. T. Phipps, J. Sanchez-Umbria, H. Schuttelaars, L. S. Tuckerman, and U. Thiele. Numerical bifurcation methods and their application to fluid dynamics: Analysis beyond simulation. *Commun. Comput. Phys.*, 15:1–45, 2014.

[7] S. Engelnkemper, S.V. Gurevich, H. Uecker, D. Wetzel, and U. Thiele. *Computational Modeling of Bifurcations and Instabilities in Fluid Mechanics*, chapter Continuation for thin film hydrodynamics and related scalar problems, pages 459–501. Computational Methods in Applied Sciences, vol 50. Springer, 2018.

[8] Y. A. Kuznetsov. *Elements of Applied Bifurcation Theory*. Springer, New York, 3rd edition, 2010.

[9] U. Thiele, A. J. Archer, M. J. Robbins, H. Gomez, and E. Knobloch. Localized states in the conserved swift-hohenberg equation with cubic nonlinearity. *Phys. Rev. E*, 87:042915, 2013.

[10] A. J. Archer, M. J. Robbins, U. Thiele, and E. Knobloch. Solidification fronts in supercooled liquids: How rapid fronts can lead to disordered glassy solids. *Phys. Rev. E*, 86:031603, 2012.

[11] A. J. Archer, M. C. Walters, U. Thiele, and E. Knobloch. Solidification in soft-core fluids: Disordered solids from fast solidification fronts. *Phys. Rev. E*, 90:042404, 2014.

[12] H. de Witt, T. Dohnal, J. Rademacher, H. Uecker, and D. Wetzel. pde2path hompage: http://www.staff.uni-oldenburg.de/hannes.uecker/pde2path/, 2019.

[13] H Uecker, D Wetzel, and JDM Rademacher. pde2path-a mat lab package for continuation and bifurcation in 2d elliptic systems. *Numer. Math.-Theory Methods Appl.*, 7:58–106, 2014.

[14] A. Pototsky, A. J. Archer, S. E. Savel'ev, U. Thiele, and F. Marchesoni. Ratcheting of driven attracting colloidal particles: Temporal density oscillations and current multiplicity. *Phys. Rev. E*, 83:061401, 2011.

[15] A. Pototsky, U. Thiele, and A. J. Archer. Coarsening modes of clusters of aggregating particles. *Phys. Rev. E*, 89:032144, 2014.